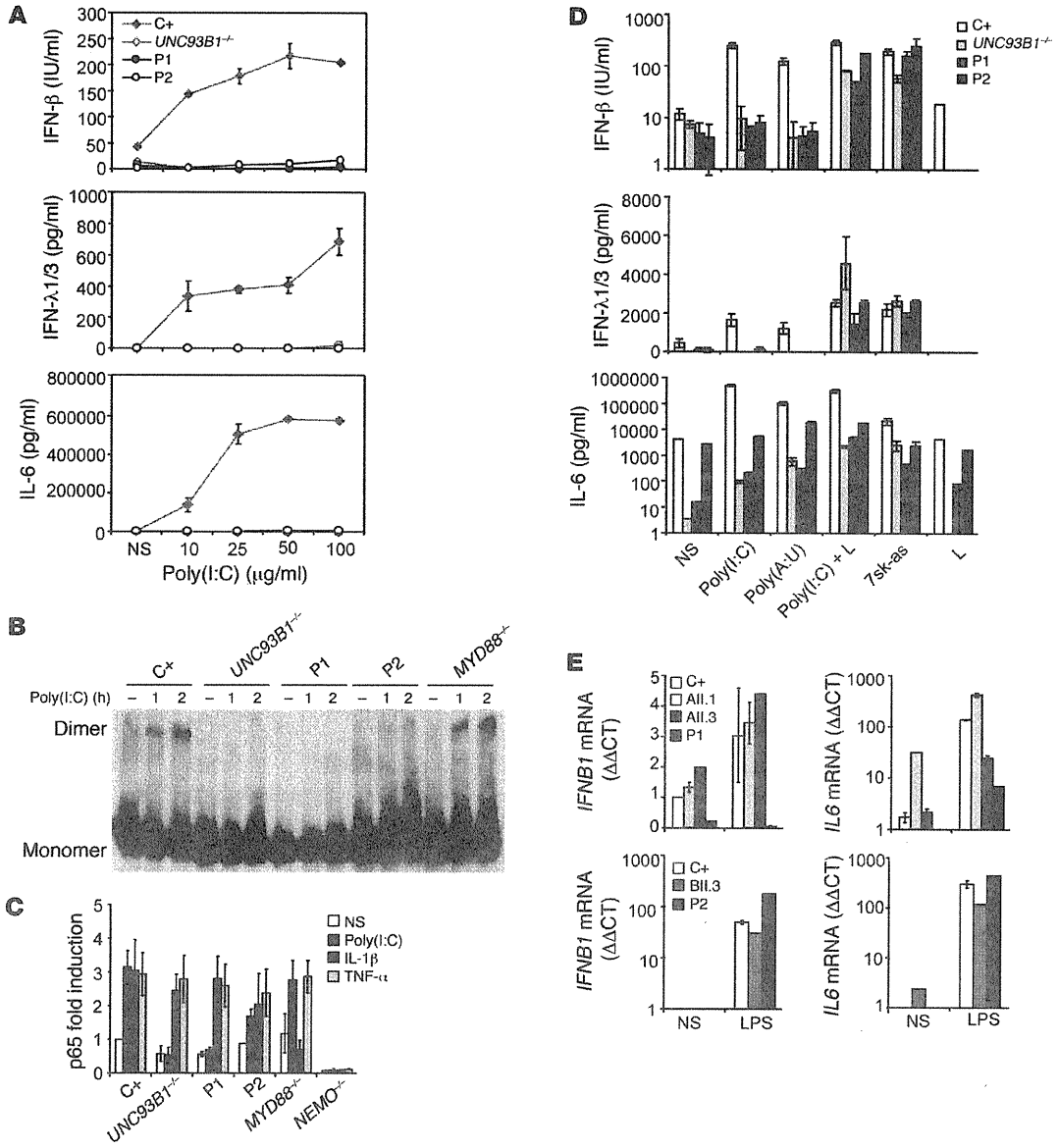

Figure 3

Response to TLR3 and TLR4 ligands. (**A**) SV40 fibroblasts were stimulated with increasing doses of poly(I:C) for 24 hours, and production of cytokines was assessed. C+ is a healthy control; *UNC93B1*$^{-/-}$ served as a negative control. Values (mean ± SEM) were calculated from 3 independent experiments. (**B**) Native gel Western blot showing IRF3 dimers from total fibroblast cell lysates after stimulation with poly(I:C) for 1 or 2 hours. C+ and *MYD88*$^{-/-}$ cells were used as positive controls to poly(I:C) stimulation, and *UNC93B1*$^{-/-}$ was used as a negative control. (**C**) Nuclear protein extracts from SV40 fibroblasts stimulated for 30 minutes with IL-1β or TNF-α and 120 minutes with poly(I:C) were tested for the presence of the p65 subunit of NF-κB by ELISA. *NEMO*$^{-/-}$ cells were used as a negative control for all stimuli; *MyD88*$^{-/-}$ was used as a negative control for IL-1β; and *UNC93B1*$^{-/-}$ was used for poly(I:C) stimulation. Values (mean ± SEM) were calculated from 3 independent experiments. NS, nonstimulated. (**D**) SV40 fibroblasts were stimulated with a TLR3-specific ligand, poly(A:U), transfected poly(I:C), RIG-I–specific ligand (7sk-as), or lipofectamine alone (L) for 24 hours and tested for cytokine production. Values (mean ± SEM) were calculated from 3 independent experiments. (**E**) PBMCs from healthy controls, various family members from kindred A (AII.1 and AII.3) and B (BII.3), and P1 and P2 were stimulated with LPS for 2 hours. Induction of *IFNB1* and *IL6* mRNA was assessed by real-time PCR. Values are expressed as relative fold change using the ΔΔCt method, where *GUS* was used for normalization; values (mean ± SEM) from 3 independent experiments were calculated.

tion by LPS in the mouse model (24–26). We therefore assessed *IFNB1* mRNA induction in response to LPS stimulation in PBMCs from the patients. Compared with those from with a healthy control or his WT or heterozygous siblings, PBMCs from P1 did not induce the production of *IFNB1* mRNA ($P < 0.05$, $P < 0.05$, and $P < 0.05$, respectively), whereas IL-6 was induced, albeit to a lower extent than in the control ($P < 0.05$), probably via the intact TLR4-MYD88–dependent pathway in P1 (Figure 3E). PBMCs from P2

and her mother, both of whom are heterozygous for the S186L mutation, were able to induce *IFNB1* and *IL6* mRNAs after LPS stimulation (Figure 3E), suggesting that the S186L *TRIF* mutation does not affect the TLR4-dependent induction of antiviral IFNs. The induction of *IFNB1* mRNA was variable among controls and subjects, but P1 was the only patient for whom no induction was observed. Consistent with this observation, results from a genome-wide transcriptional analysis of the TLR4 pathway in PBMCs of a control, P1, and an AR MyD88-deficient patient showed impaired responses to LPS in P1 (Supplemental Figure 5A), although P1 responded normally to the TLR7/8 ligand R848 unlike the MyD88-deficient cells (Supplemental Figure 5B). As expected, MyD88-deficient cells did not respond normally to LPS, and a different pattern of LPS dysregulation was observed in the MyD88-deficient cells when compared with that in cells from P1, demonstrating the distinct pathways involved in the TLR4-MyD88 dependent pathway (Supplemental Figure 5, A and C). We found that the functional pathways regulated by LPS in control PBMCs consisted of genes involved in the production of various cytokines (*IFNB1*, *IL23A*, *IL19*, *IL1A*, and *IL1F9*), chemokine-related genes (*CCR1*, *CCL3L1*, *CCL3L3*, *CCL14*, *CCL20*, and *CCL23*), and IFN-regulated genes (*IFIT3* and *IRF8*) (Supplemental Figure 5C). The nonsense mutation in P1 is consistent with a null mutation affecting all aspects of TRIF-specific signaling, including TLR4-TRIF responses. By contrast, the collective data for the kindred carrying a missense TRIF allele point to a specific defect in the TLR3 signaling pathway, suggesting that the TRIF missense allele is dysfunctional and dominant for TLR3 but not TLR4 responses and for the induction of antiviral IFNs in particular.

Impaired cellular responses to viruses. We then assessed the responses of fibroblasts to viral infection. P1 and P2 cells showed impaired production of IFN-β, IFN-λ1/3, and IL-6 upon infection with VSV and HSV-1, like UNC-93B–deficient cells and unlike control cells ($P < 0.05$ for all comparisons) (Figure 4, A and D). Cell viability after infection with VSV and HSV-1 was tested in the presence and absence of exogenous IFN-α (Figure 4, B and E). In control cells, there was a small decrease or no decrease in the number of living cells upon infection with VSV or HSV-1, respectively. However, cells from P1 and P2 both had significantly lower percentages of surviving cells as compared with those of control cells, at MOIs of 10–100 with VSV ($P < 0.05$ for all comparisons) and upon HSV-1 infection ($P < 0.05$ for all comparisons). However, the addition of exogenous IFN-α resulted in very little cell death in cells from either P1 or P2, in contrast with what was observed for STAT1-deficient cells, which were unable to respond normally to IFN-α. This is consistent with the higher VSV viral titers in P1 and P2 compared with those in a healthy control ($P < 0.05$ for both comparisons), which were reduced to control levels after pretreatment with IFN-α (Figure 4C). Similarly, both P1 and P2 showed higher levels of HSV-1 replication compared with those of a control, which was also reduced with the addition of IFN-α (Figure 4F). Thus, the susceptibility of P1 and P2 to viruses probably results from a lack of protective endogenous IFN-α/β and/or IFN-λ production during viral infection. These data suggest that both P1 and P2 harbor a specific defect in the TLR3-dependent induction of IFN-β and IFN-λ, in response to HSV-1 and VSV, resulting in enhanced viral growth and cell death, at least in fibroblasts. This phenotype is consistent with those reported for both UNC-93B and TLR3 deficiencies and suggests that the R141X and S186L *TRIF* alleles are deleterious, with complete cellular penetrance but incomplete clinical penetrance (10, 11).

Functional characterization and complementation of the R141X mutation. We further investigated the impact of the R141X nonsense mutation by transiently transfecting 293HEK-TLR3 cells, which are responsive to poly(I:C) stimulation, with WT, R141X, or ΔNC TRIF constructs. The ΔNC TRIF construct encodes a truncated dominant-negative TRIF, consisting of only the 162 amino acids of the TIR domain (20). As expected, the R141X TRIF plasmid did not induce expression from the IFN-β or NF-κB promoters, unlike the WT plasmid, as shown by luciferase assays (Figure 5A). The level of induction was similar to that of cells transfected with empty plasmids, consistent with a null allele, and contrasting with the dominant-negative effect observed with the ΔNC plasmid. When the cells were transfected with equal amounts of WT plasmid and R141X or ΔNC, lower levels of luciferase activity were observed only in WT/ΔNC cells, suggesting that the R141X allele does not exert a dominant-negative effect. By contrast to what was observed with cells from P1, analysis of the proteins produced by transfected cells revealed the presence of an approximately 15-kDa truncated R141X protein (Figure 5B). The induction of the IFN-β promoter in response to LPS is strictly TRIF dependent. We therefore transiently transfected LPS-responsive 293HEK-TLR4-MD2-CD14 cells with the TRIF plasmids (Figure 5C). The R141X plasmid, unlike the WT plasmid, did not induce luciferase gene expression from the IFN-β plasmid, and cotransfection with the WT plasmid did not decrease luciferase induction, consistent with a null effect. However, the R141X and mock plasmids were able to induce NF-κB after LPS stimulation in these cells, as the induction of the NF-κB promoter is primarily MyD88 dependent, consistent with the known role of TRIF in TLR4 signaling. Transient transfection of control fibroblasts or fibroblasts from the patient with WT TRIF cDNA led to rapid apoptosis (data not shown), as previously shown in other systems (33, 34). Complementation of the patient's fibroblast phenotype was therefore achieved by retroviral transduction. A doxycycline-regulated *TRIF* expression vector was used for the retroviral transduction of fibroblasts from P1, such that *TRIF* expression was repressed in the presence of doxycycline, making it possible to obtain stably transduced clones (Supplemental Figure 6A). The transduction of cells from P1 with the WT TRIF plasmid (P1+WT) restored poly(I:C)-induced IFN-β, IFN-λ, and IL-6 production, whereas cells transduced with the R141X plasmid (P1+R141X) remained unresponsive (Figure 5D). Viral replication after HSV-1 infection was also rescued in P1+WT cells but not in P1+R141X cells (Figure 5E). Thus, the R141X mutation in P1 is responsible for TRIF deficiency and the abolition of TLR3 signaling as well as susceptibility to HSV-1.

Functional characterization of the S186L mutation in 293-TLR3 cells. The molecular mechanism by which the S186L *TRIF* mutation exerts its deleterious effects was then investigated. We transfected 293-TLR3 cells with expression plasmids encoding WT or S186L TRIF. Reporter assays were performed with the IFN-β and NF-κB–luciferase constructs. In WT and S186L *TRIF*-transfected cells, marked induction of IFN-β and NF-κB luciferase was observed in the absence of poly(I:C) stimulation, consistent with previous reports in which *TRIF* overexpression led to TLR3-independent activation of IFN-β and NF-κB (Figure 6A, Supplemental Figure 7A, and refs. 21, 25). We assessed the ability of these mutations to interact with TLR3 upon poly(I:C) stimulation by transfecting 293-TLR3 cells with the mutant plasmids and the IFN-β luciferase construct and then stimulating them with poly(I:C) (Supplemental Figure 7B). Transfection with the S186L allele resulted in the induction of

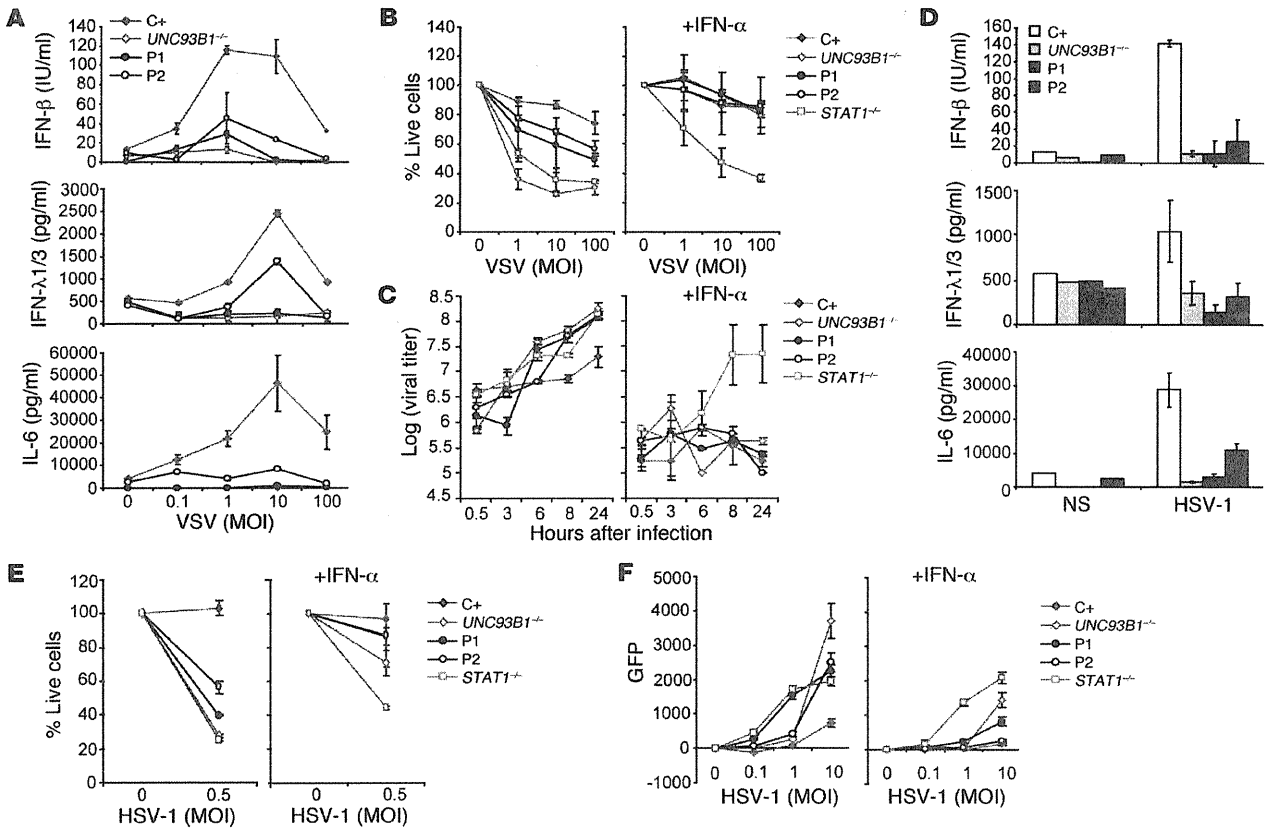

Figure 4

Response to viral infections. (**A**) IFN-β, IFN-λ1/3, and IL-6 production in SV40 fibroblasts 24 hours after infection with VSV. Values (mean ± SEM) were calculated from 3 independent experiments. (**B**) Cell viability of SV40 fibroblasts after 24 hours of infection with VSV in the absence (left) or presence (right) of recombinant IFN-α. The percentage of surviving cells was assessed using resazurin. C+ is a healthy control; *UNC93B1*$^{-/-}$ and *STAT1*$^{-/-}$ cells were used as negative controls. Values (mean ± SEM) were calculated from 3 independent experiments. (**C**) VSV replication in SV40 fibroblasts was estimated at various time points after infection using an MOI of 10. Cells were pretreated with IFN-α or media alone. VSV titer estimation was carried out on Vero cells. Values (mean ± SEM) were calculated from 3 independent experiments. (**D**) IFN-β, IFN-λ1/3, and IL-6 production after infection with 1 MOI of HSV-1 in SV40 fibroblasts after 24 hours. Values (mean ± SEM) were calculated from 3 independent experiments. (**E**) Cell viability of SV40 fibroblasts was assessed using resazurin after 24 hours of HSV-1 infection. C+ is a healthy control; *UNC93B1*$^{-/-}$ and *STAT1*$^{-/-}$ cells were used as negative controls. Cells were pretreated with media (left) or recombinant IFN-α (right). Values (mean ± SEM) were calculated from 3 independent experiments. (**F**) Replication of HSV-1 GFP was assessed in SV40 fibroblasts after 24 hours of infection. Cells were pretreated with media (left) or recombinant IFN-α (right). Values (mean ± SEM) were calculated from 3 independent experiments.

IFN-β upon poly(I:C) stimulation, as observed for the WT TRIF plasmid. After activation by TLR3, TRIF forms homo-oligomers in the cytosol that are responsible for all downstream signaling events (29). These homo-oligomers may be visualized on confocal microscopy as speckle-like structures. Activated TRIF was observed in HeLa cells after poly(I:C) stimulation in cells transfected with the WT or S186L plasmid, suggesting that mutant TRIF was able to interact with TLR3 and homo-oligomerize, like WT TRIF (Supplemental Figure 7C and ref. 29). Data for transient transfection with the S186L allele revealed no difference between the functions of this mutant form and the WT TRIF. The effect of this mutation was undetectable in transient transfection experiments, even if carried out with as little as 10 pg plasmid (data not shown).

Investigating TRIF overexpression in transient transfection. We then addressed the issue of the dominance of the S186L allele. However, as the hypomorphic mutation alone demonstrated normal TRIF function, cotransfection of WT and S186L alleles also revealed normal activation comparable to WT TRIF in 293-TLR3 cells (data not shown). We hypothesize that TRIF levels were already saturated in transient transfection experiments and were therefore not sensitive enough to reveal subtle differences. One of the problems inherent to studies of TRIF overexpression is that the protein is constitutively active and induces apoptosis (20, 33, 34), which does not occur in cells producing small amounts of endogenous TRIF. Indeed, TRIF is normally produced in very small amounts in cells, only transducing and recruiting downstream signaling molecules upon stimulation by TLR3 (29, 35). Thus, the amounts of TRIF protein produced in conditions of overexpression do not reflect physiologically relevant functions of TRIF, as they cause constitutive activation and apoptosis. The transient transfection system has been successfully used by many groups to study the function of TRIF in conditions of overexpression (20, 21, 28, 29,

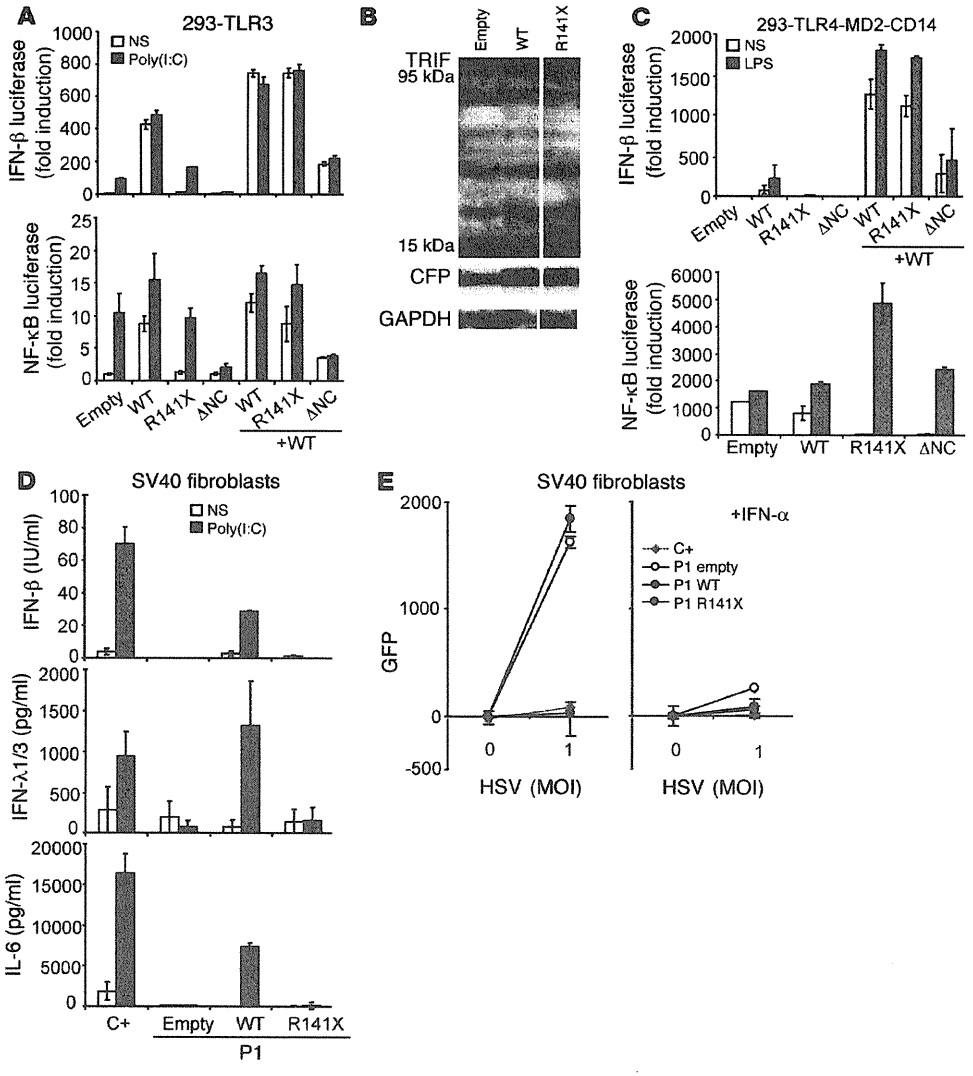

Figure 5

Molecular characterization of the R141X AR TRIF mutation. (**A**) 293 HEK-TLR3 cells were transfected with 10 ng empty vector, WT, R141X, or ΔNC TRIF along with IFN-β–Luc/NF-κB–Luc and RL-TK vectors to assess induction upon overexpression of TRIF. ΔNC TRIF serves as a dominant-negative construct of TRIF, containg only the TIR domain. Transfected cells were left unstimulated or stimulated with 50 μg/ml poly(I:C) for 4 hours. Firefly luciferase values were normalized using renilla values. Total transfected DNA was held constant by adding empty vector. Values (mean ± SEM) were calculated from 3 independent experiments. (**B**) Immunoblot analysis of protein lysates from 293HEK-TLR3–transfected cells, using an antibody recognizing the N-terminal of TRIF. CFP was cotransfected as a control for transfection efficiency. Samples were migrated on the same blot. (**C**) 293HEK-TLR4-MD2-CD14 cells were transfected with 10 ng TRIF vectors, including WT, R141X, and ΔNC TRIF, and the induction of IFN-β–Luc/NF-κB–Luc was assessed by luciferase. Values (mean ± SEM) were calculated from 3 independent experiments. (**D**) Control (C+) SV40 fibroblasts and P1's fibroblasts retrovirally transduced with empty vector, WT TRIF, or R141X TRIF were stimulated with 25 μg/ml poly(I:C) for 24 hours, and production of cytokines was assessed by ELISA. Values (mean ± SEM) were calculated from 3 independent experiments. (**E**) HSV-1 GFP replication was assessed after 24 hours of infection in control SV40 fibroblasts (C+) and SV40 fibroblasts from P1 retrovirally transduced with empty vector, WT, or R141X TRIF. Cells were pretreated with media (left) or recombinant IFN-α (right). Values (mean ± SEM) were calculated from 3 independent experiments.

33, 36). However, a review of the literature showed that no study has ever demonstrated a hypomorphic effect of a point mutation in the context of this transfection system; only null effects have been characterized. These findings support the notion that subtle effects cannot be studied accurately in the context of overexpression.

Functional characterization of the S186L allele in retroviral transduced fibroblasts. We then made use of the fibroblasts available from the patient with AR TRIF deficiency (P1) for retroviral transfection experiments with the S186L allele. Retroviral transduction yielded much lower TRIF levels, although these levels were nonetheless higher than endogenous levels (Supplemental Figure 6). The lack of constitutive activation in retrovirally transduced cells (Figure 5D and Figure 6, B and C) and the low levels of apoptosis suggest that TRIF levels in this system were similar to endogenous levels. They may, therefore, provide ideal conditions for the detection of subtle mutations. The S186L-transduced cells (P1+S186L cells) resulted in significantly lower levels of cytokine production in response to poly(I:C) stimulation compared with P1+WT cells ($P < 0.05$ for all comparisons), suggesting that the S186L allele is hypomorphic (Figure 6B and Supplemental Figure 6A). Furthermore, complementation of fibroblasts from P2, which express endogenous *TRIF*, was achieved with the WT TRIF allele (P2+WT), whereas the S186L allele (P2+S186L) showed impaired responses in terms of the production of IFN-β, IFN-λ, and IL-6 compared with P2+WT cells ($P < 0.05$ for all comparisons) (Figure 6C and Supplemental Figure 6B). Moreover, viral replication after HSV-1 infection in P1+WT cells was comparable to that of a control, whereas P1+S186L cells had significantly higher viral titers compared with those of a control or with P1+WT cells ($P < 0.05$ for both comparisons). There was lower replication in P1+S186L cells than in cells from P1 retrovirally transduced with empty vector (P1+Empty cells) ($P < 0.05$), consistent with a hypomorphic effect (Figure 6D).

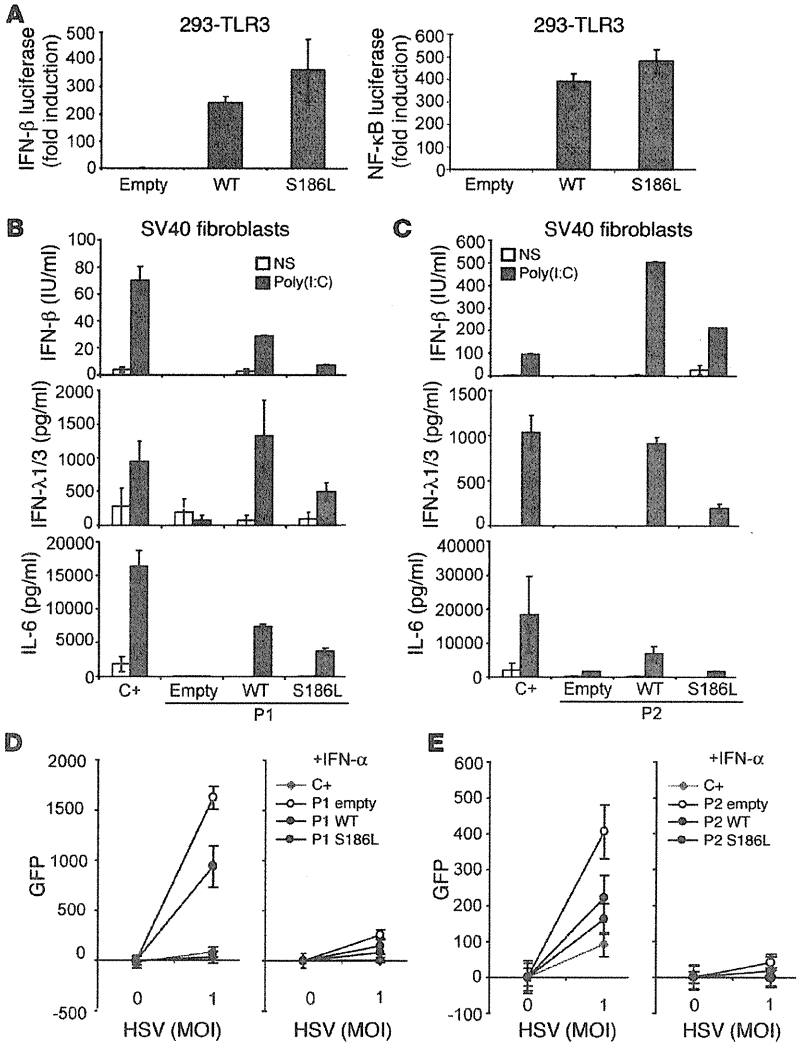

Figure 6
Functional characterization of the S186L AD TRIF mutation. (**A**) 293HEK-TLR3 cells were transfected with empty vector, WT, or S186L TRIF plasmids along with IFN-β–Luc/NF-κB–Luc and RL-TK vectors to assess IFN-β and NF-κB promoter induction upon overexpression of TRIF. Values (mean ± SEM) were calculated from at least 3 independent experiments. (**B**) SV40 fibroblasts from control (C+) and P1's fibroblasts retrovirally transduced with either empty vector, WT TRIF, or S186L TRIF were stimulated with 25 μg/ml poly(I:C) for 24 hours, and the production of cytokines was assessed by ELISA. Values (mean ± SEM) were calculated from at least 3 independent experiments. (**C**) SV40 fibroblasts from control (C+) and P2's fibroblasts retrovirally transduced with empty vector, WT TRIF, or S186L TRIF were stimulated with 25 μg/ml poly(I:C) for 24 hours, and the production of cytokines was assessed by ELISA. Values (mean ± SEM) were calculated from at least 3 independent experiments. (**D**) Replication of HSV-1 GFP was assessed after 24 hours of infection in control SV40 fibroblasts (C+); SV40 fibroblasts from P1 retrovirally transduced with empty vector, WT, or S186L TRIF; and (**E**) SV40 fibroblasts from P2 retrovirally transduced with empty vector, WT, or S186L. Cells were pretreated with media (left) or recombinant IFN-α (right). Values (mean ± SEM) were calculated from at least 3 independent experiments.

Increased HSV-1 replication observed in P2+Empty cells was also complemented in P2+WT cells ($P < 0.05$) (Figure 6E). P2+S186L cells showed a trend toward higher HSV-1 titers compared with that of P2+WT cells, although the difference was not statistically significant, which can be attributed to the hypomorphic nature of the S186L allele. Overall, these data suggest that the S186L mutation is hypomorphic, affecting both the IRF3/IFN-β and NF-κB/IL-6 pathways and controlling susceptibility to HSV-1 infection.

A heterozygous nondeleterious TRIF missense mutation in P3. We identified a third distinct heterozygous mutation in *TRIF* in a boy of Iranian origin (P3), who was born to nonconsanguineous parents and who suffered from HSE at 4.5 years of age (Supplemental Figure 8A). The patient is now 7 years old and has not suffered from other unusual or severe infections. Mutations in the coding regions of *UNC93B1*, *TLR3*, and *TRAF3* were excluded. Further sequencing of leukocyte gDNA from P3 lead to the discovery of a heterozygous missense mutation in TRIF at nucleotide position 1875 (c.1875C>T), resulting in a leucine at amino acid residue 625 in place of a proline in the proline-rich domain of the C terminus of TRIF (P625L) (Supplemental Figure 8, B and C). This mutation was inherited from P3's father who is seronegative for anti–HSV-1 antibodies; hence, P3 remains the only family member affected by HSE. This mutation was not found in the NCBI database, the 1,050 unrelated healthy controls from the CEPH-HGD panel, or in an additional 109 healthy Iranian controls tested, confirming that c.1875C>T is a not a polymorphism. Proline at position 625 was conserved in 7 out of the 11 animal species in which TRIF shares over 50% homology with human TRIF (Supplemental Figure 8D). TRIF protein and mRNA expression were normal in EBV-B cells from P3 (Supplemental Figure 8E and data not shown). This mutation occurred in the proline-rich C-terminal region, implicated in homo-oligomerization, RIP1 binding, NF-κB activation, and apoptosis-inducing functions of TRIF (29, 33). However, despite a poly(I:C) nonresponsive fibroblast phenotype (Supplemental Figure 8F), we did not observe complementation of the phenotype by retroviral transduction of the WT TRIF allele in P3's cells (Supplemental Figure 8H). Moreover, P3's mutation P625L transduced into P1's cells did not differ from WT TRIF–transduced cells in its ability to induce cytokines after poly(I:C) stimulation (Supplemental Figure 8F and Supplemental Figure 6A). Hence, although not found in healthy controls, we were unable to show that this particular mutation is deleterious with the assays available. We hypoth-

esize that P3 carries a pathogenic mutation affecting another gene in the TLR3 signaling pathway. These data neatly illustrate the importance of careful functional characterization of rare mutant alleles, as shown for P2, to ascribe disease responsibility.

Discussion

We report here the first 2 kindreds with AR and AD TRIF deficiencies conferring a predisposition to childhood HSE to our knowledge. The loss-of-expression, loss-of-function, nonsense R141X allele results in the abolition of TLR3-mediated signaling and TRIF-dependent TLR4 responses in the cells of P1. Most family members of P1 are heterozygous carriers of this mutation but have not suffered from HSE or any other infection otherwise. Despite diminished TRIF protein in cells from heterozygous individuals, their leukocytes responded to LPS by the induction of IFN-β transcripts, suggesting that TRIF function was maintained. Moreover, the R141X allele was not dominant negative in 293-TLR3 transfection assays. We did not have access to heterozygous fibroblasts for further testing of the TLR3 pathway, but these results suggest that this defect is purely recessive and that there is no cellular or clinical haploinsufficiency at the *TRIF* locus. The TLR4-TRIF pathway was the only TIR pathway for which no inborn defect had been detected, as it is not defective in patients with UNC-93B, TLR3, MYD88, and IRAK4 deficiencies (10, 11, 13, 37–40). The amounts of IFN-α/β produced in response to the human TRIF-dependent TLR4 pathway are modest, and the role of this pathway in host defense has remained elusive (41, 42). The identification of complete TRIF deficiency in P1, who did not suffer from any infection other than HSE, opportunistic or otherwise, suggests that the human TLR4-TRIF pathway is largely redundant in host defense. Moreover, our study suggests that the recently described role of TRIF in DExD/H-box helicases-dependent cytosolic pathways is also probably redundant for protective immunity (27).

We also identified a patient, P2, with a heterozygous missense mutation in the N-terminal region of TRIF (S186L), defining AD TRIF deficiency as a genetic etiology of HSE. Cells from P2 displayed impaired TLR3-mediated signaling but the maintenance of TRIF-dependent TLR4 responses. The mutant allele showed complete penetrance at the cellular level, because fibroblasts from the 2 TRIF heterozygotes tested, P2 and her mother, showed impaired TLR3 responses. The N-terminal region of TRIF, including the TBK1-binding domain, is indispensable for the IRF3 pathway, consistent with the cellular phenotype of P2, in which IFN-β production and IRF3 dimerization were more affected than the production of IL-6 and NF-κB nuclear translocation after poly(I:C) stimulation (21, 25, 36). P2 fibroblasts were rescued by the WT — but not the mutant TRIF — allele, indicating that the allele is deleterious. The S186L allele appeared functional when used for the transient transfection of 293-TLR3 cells, whereas it was dysfunctional when introduced by retroviral transduction into TRIF-deficient fibroblasts from P1, suggesting that it is hypomorphic but not a complete loss-of-function allele. Data for the kindred with AR complete TRIF deficiency suggest that there is no haploinsufficiency at the *TRIF* locus, pointing toward the notion of the S186L mutation being dominant negative. However, it was difficult to determine experimentally whether the S186L allele was actually dominant negative, as overexpressed TRIF is constitutively active and a potent inducer of apoptosis, preventing fine analysis of the TLR3 pathway. Nonetheless, the available data suggest that the hypomorphic S186L allele of TRIF is probably dominant negative and responsible for AD TRIF deficiency and HSE.

The clinical penetrance of AR TRIF deficiency appears, so far, to be complete, as only one patient with this deficiency has been identified and has had HSE. Similarly, the only known patients with AR TLR3 or AD TRAF3 deficiency also show complete clinical penetrance (12, 13). In contrast, the penetrance of AD TRIF deficiency is incomplete, as only 1 out of the 3 S186L TRIF heterozygotes developed HSE upon infection with HSV-1. This is consistent with AR UNC-93B and AD TLR3 deficiencies, which also show incomplete clinical penetrance (10, 11). Whole-exome sequencing carried out in P2 failed to identify overt deleterious mutations that may explain the variable penetrance (data not shown). In patients with mutations in any of these 4 genes, HSE probably resulted from the impairment of antiviral IFN production in the CNS, leading to higher levels of viral replication and the death of resident cells. The fibroblastic and clinical phenotypes of AR and AD TRIF deficiencies are strikingly similar to those of UNC-93B deficiency (10), TLR3 deficiency (11, 13), and TRAF3 deficiency (12), consistent with the known role of TRIF as the sole adaptor for TLR3. This identification of a fourth gene underlying susceptibility to HSE in 2 kindreds is consistent with our model for the genetic architecture of infectious diseases (18, 43). We proposed that life-threatening pediatric infectious diseases can result from the inheritance of rare single gene mutations, highly deleterious at the cellular level but of variable clinical penetrance (18, 44). Although unlikely, the lack of infectious phenotype or the selective susceptibility to HSE observed in known patients with inborn errors of TLR3 immunity might result from compensatory variations at other loci. The TLR3 pathway is vital for protection against HSE, at least in some children, which may additionally ensure that chronic latency of HSV-1 heightens immunity against other microbes, as shown in the mouse model (45). In any case, HSE provides proof of principle that a collection of single-gene variations displaying incomplete penetrance at the clinical level and affecting different but immunologically related genes may account for severe, sporadic, and common infectious diseases of childhood.

Methods

Patients

We investigated 3 unrelated patients who suffered from HSE during childhood. P1 is a Saudi Arabian boy of consanguineous parents (first cousins). There is no family history of encephalitis, and there was no remarkable infectious history until P1 developed viral meningitis of unknown origin at 1.5 years of age. At the age of 2, he developed HSE, presenting with irritability, fever, and partial seizure. HSE was confirmed by a positive PCR for HSV-1 in the CSF. An MRI scan showed atrophy of the left temporal lobe, and an EEC revealed epileptogenic activity. He suffers from neurological sequelae, mainly consisting of delayed speech. He also has recurrent herpetic stomatitis. He has not yet been exposed to other herpes viruses, determined by negative serology for CMV and VZV.

P2 is a French, Swiss, and Portuguese girl, of nonconsanguineous parents. There is no family history of encephalitis. The mother suffered from meningitis of unknown origin at the age of 9, from which she fully recovered. The mother and maternal grandmother have had herpes labialis. The mother, the maternal grandfather, and P2 are all seropositive for HSV-1. Of note, P2 had a rectovaginal fistula surgical intervention at birth. There was no remarkable infectious history until P2 suffered from serologically determined HSE at 21 months, presenting with high fever. HSE was confirmed

by a positive PCR for HSV-1 in the CSF. Serum analysis detected recent HSV-1 seroconversion. Treatment with acyclovir was administered 4 days after symptoms of fever, after which the patient was hospitalized for treatment. There was no relapse, and she has never suffered from herpes labialis. She suffers from neurological sequelae, mainly consisting of blindness and epilepsy. Following HSE, she has been exposed to other herpes viruses, as shown by positive serology for VZV and EBV with no complications. She has been vaccinated with MMR with no adverse effects.

P3 is an Iranian boy of nonconsanguineous parents. P3 presented with fever, vomiting, and convulsions, with right temporal involvement as shown by MRI. HSE diagnosis was confirmed by an HSV-1–positive PCR in the CSF. Treatment was initiated with acyclovir with no significant improvement. Subsequent treatment with foscarnet for 21 days was successful. At day 23, symptoms of low consciousness and choreatic movement were observed along with a positive PCR for HSV-1. Treatment with cidofovir was administered for 5 days, and he has fully recovered. P3 has not yet been exposed to other herpes viruses, such as VZV and EBV, as determined by negative serology. Of note, the father who carries the mutation is seronegative for serum antibodies to HSV, whereas the mother is seropositive. There is no remarkable medical history in the family.

Cell lines

Skin biopsy specimens from the patients as well as family members, the UNC-93B–deficient patient, TLR3-deficient patient, the MyD88-deficient patient, the STAT1-deficient patient, and healthy controls were obtained for the establishment of primary fibroblasts. Primary fibroblasts were cultured in DMEM supplemented with 10% FBS, 10 U/ml penicillin, 10 μg/ml streptomycin, and 62.5 ng/ml amphotericin B (Invitrogen). Fibroblasts were immortalized with the SV40 large T antigen, as previously described (46). NEMO-deficient immortalized fibroblasts were derived from a fetus with incontinentia pigmenti (47). All cell lines were incubated at 37°C, under an atmosphere containing 5% CO_2. PBMCs from patients and healthy controls were harvested from fresh blood by Ficoll-Hypaque density gradient centrifugation (GE Healthcare). PBMCs were cultured in RPMI supplemented with 10% FBS (Invitrogen) or 1% human sera.

Activation by TLR ligands

A synthetic analog of dsRNA, poly(I:C) (TLR3 agonist, at 25 μg/ml), and LPS (LPS *Salmonella minnesota*, TLR-4 agonist, at 10 to 100 ng/ml) were purchased from Invivogen; resiquimod hydrochloride (R-848; TLR-7, and TLR-8 agonist, at 3 μg/ml) was purchased from GLSynthesis Inc.; unmethylated CpG DNA CpG-A (D19) (TLR-9 agonist, at 5 μg/ml) was provided by Robert Coffman and Frank Barrat (both from Dynavax Technologies, Berkeley, California); and IL-1β (at 20 ng/ml) and TNF-α (at 20 ng/ml) were obtained from R&D Systems. All agonists and reagents were endotoxin free. In all stimulations of PBMCs with TLR agonists other than LPS, the cells were incubated with 10 μg/ml polymyxin B (Sigma-Aldrich), at 37°C, for 30 minutes before activation. TLR agonists were used to stimulate PBMCs for 48 hours, at a concentration of 2×10^6 cells per ml in RPMI 1640 supplemented with 10% FBS or 1% human serum. The SV40-fibroblast cell lines were activated in 24-well plates, at a density of 10^5 cells per well, for 24 hours with poly(I:C) (25 μg/ml), TNF-α (20 ng/ml), IL-1β (20 ng/ml), IPH 3102 or poly(A:U) (50 μg/ml) TLR3-specific ligand (Innate Pharma), and 7sk-as (provided by Caetano Reis e Sousa, London Research Institute, London, United Kingdom).

Viral infections for cytokine determination

PBMCs isolated by Ficoll-Paque density gradient centrifugation were stimulated with various intact viruses for 24 hours, at a density of 2×10^6 cells per ml in RPMI 1640 supplemented with 10% FBS or, for some experiments, 2% FBS. The following viruses were used: the dsDNA virus HSV-1 (KOS-1 strain, MOI = 1) and the ss(–)RNA virus VSV (Indiana strain, MOI = 1). The SV40-fibroblast cell lines were activated in 24-well plates, at a density of 10^5 cells per well, for 24 hours with HSV-1 or VSV. Cell supernatants were recovered and tested for cytokine production by ELISA.

Cytokine determinations

The production of IFN-α, IFN-β, IFN-λ1/3, and IL-6 was assessed by ELISA, according to the kit manufacturer's instructions, respectively: Human IFN-α Module Set (AbCys SA), Human IFN-β ELISA Kit (TFB, Fujirebio Inc.), Duo Set Human IL29/IL28B (IFN-λ1/3) (R&D Systems), and Human IL-6 (Sanquin).

Q-PCR

Total RNA was extracted from cells either unstimulated or stimulated with TLR agonists. All RNA samples were treated with RNase-free DNase (Qiagen) after isolation with the RNeasy Extraction Kit (Qiagen). RNA was reverse transcribed directly, with the High Capacity RNA-to-cDNA Master Mix (Applied Biosystems). Q-PCR was performed with Applied Biosystems Assays-on-Demand probe/primer combinations specific for IFN-β, IL-6, TRIF, and β-glucuronidase (GUS), which was used for normalization. Results are expressed according to the ΔΔCt method, as described by the manufacturer.

Western blots

Total cell extracts were prepared from 293-NULL, 293-TLR3, 293-TLR4-MD2-CD14, SV40 fibroblasts, and EBV-B cells. Equal amounts of protein from each sample were separated on SDS-PAGE gels and blotted onto iBLOT gel transfer stacks (Invitrogen), which were then probed with antibodies and developed with peroxidase-conjugated secondary antibodies and ECL Western blotting substrate (GE Healthcare). TRIF antibodies binding to the N-terminal region of human TRIF (Alexis Biochemicals) were used for Western blots. Anti-CFP (Abcam), anti-ACTIN, anti-GAPDH (Santa Cruz Biotechnology Inc.), and anti-HA antibodies (Sigma-Aldrich) were also used.

Signal transduction studies

Nuclear cell extracts were prepared from SV40-fibroblasts after incubation with or without poly(I:C), TNF-α, and IL-1β. TransAM NF-κB p65 ELISA (Active Motif) was performed with an NF-κB p65-specific DNA probe and 10 μg nuclear extract. The Bio-Rad protein assay was used to determine protein concentrations. For the detection of IRF3 dimerization, whole-cell extracts were prepared from SV40-fibroblasts with or without poly(I:C) treatment. The IRF3 monomers and dimers were separated by native PAGE in the presence of 1% sodium deoxycholate (DOC) (Sigma-Aldrich). Total cell extracts (25 μg of protein) were diluted 1:2 in nondenaturing sample buffer (125 mM Tris-HCl, pH 6.8, 30% glycerol, and 2% DOC) and separated by electrophoresis in a 7.5% polyacrylamide gel, in 25 mM Tris and 192 mM glycine, pH 8.4, with 1% DOC present in the cathode chamber only. The gel was blotted onto a membrane, which was then probed with the anti-IRF3 antibody (FL-425, Santa Cruz Biotechnology Inc.).

Transient transfections and reporter assays

The mutant alleles were generated with the QuikChange II Site-Directed Mutagenesis Kit from Qiagen for introduction of the C421T, C557T, and C1875T mutations into the pEF-Bos-TRIF plasmid C-terminally tagged with HA (provided by Misako Matsumoto). The pcDNA3-CFP vector (Addgene) was used to control for transfection efficiency. The ΔNC TRIF construct was a gift from Osamu Takeuchi (Osaka University, Osaka, Japan). pGL4.32[*luc2P*/NF-κB-RE/Hygro] NF-κB luciferase and pRL-TK *Renilla*

luciferase plasmids were purchased from Promega Corporation. The IFN-β promoter-luciferase construct was provided by Christopher Basler (Mount Sinai School of Medicine, New York, New York, USA). 293-NULL, 293-hTLR3, or 293-hTLR4A-MD2-CD14 cells (Invivogen) were plated in 24-well plates and transfected with the expression vectors in the presence of lipofectamine LTX reagent, according to the manufacturer's instructions (Invitrogen). The total amount of DNA was kept constant with empty vector (1 μg/well). Apoptosis was inhibited by adding 20 μM z-VAD-fmk (Sigma-Aldrich) to each well. Twenty hours after transfection, the cells were incubated for 4 hours more, with or without 50 μg/ml poly(I:C). Cell lysates were obtained and analyzed with the Dual-Luciferase Reporter Assay System (Promega Corporation), according to the manufacturer's instructions. Firefly luciferase values were normalized against *Renilla* luciferase activity and expressed as fold change with respect to cells transfected with the empty vector.

Confocal microscopy

HeLa cells were transfected with the expression plasmid for WT TICAM-1 (WT) or the S186L mutant (0.2 ng); 24 hours after transfection, cells were stimulated with buffer alone or with 10 μg/ml poly(I:C) for 30 minutes. Cells were fixed in 4% paraformaldehyde for 30 minutes and permeabilized with 0.2% Triton X-100 in PBS for 10 minutes. Fixed cells were blocked in 1% bovine serum albumin in PBS and labeled by incubation with anti-HA pAb for 60 minutes at room temperature. Alexa Fluor 594–conjugated secondary antibodies (1:400) were used to visualize the primary antibody. Nuclei were stained with DAPI (2 μg/ml) in PBS for 10 minutes, before being mounted on glass slides in PBS supplemented with 2.3% 1,4-diazabicyclo[2.2.2]octane and 50% glycerol. Cells were visualized at ×63 magnification, with an LSM510 META microscope (Zeiss).

Retroviral transduction of SV40 fibroblasts

The doxycycline-inducible expression plasmid (pLINX-Flag) and pLINX-Flag-TRIF were provided by Sang Hoon Rhee (UCLA, Los Angeles, California, USA). The C421T, C557T, and C1875T mutations were introduced into the pLINX-Flag-TRIF plasmid by site-directed mutagenesis, as described above. 293T cells (ATCC no. CRL-11268) were grown in DMEM (Gibco BRL/Invitrogen) supplemented with 10% heat-inactivated FBS, 50 IU/ml penicillin, and 50 μg/ml streptomycin (Gibco BRL/Invitrogen) at 37°C in a humidified atmosphere containing 5% CO_2. Retroviral vectors pseudotyped with the vesicular stomatitis G protein (VSV-G) were generated as previously described (48) by calcium phosphate transfection into 293T cells of a packaging construct, pMNold gag-pol; a plasmid producing the VSV-G envelope (pMD.G); and each of the pLINX vectors. Culture medium was collected at 24, 48, and 72 hours, pooled, 0.45-μ filtered, and concentrated approximately 1,000 fold by ultracentrifugation. Fibroblasts (1.5×10^5 cells per well) were seeded into a 12-well dish and infected on the following day, with 8 to 16 μl of each retroviral vector for 4 hours. Twenty-four hours later, the medium was replaced with DMEM containing 1 μg/ml doxycycline (Clonetech) to prevent expression of the TRIF cDNA insert. Forty-eight hours later, DMEM containing doxycycline and 1 mg/ml G418 (Invivogen) was added to the cells. Selected cells were amplified. The stably transduced cells were then plated in 24-well plates without doxycycline for 24 hours and stimulated with 25 μg/ml poly(I:C) for an additional 24 hours. The cells were lysed after 48 hours of culture in the absence of doxycycline.

Viral replication

For viral titration of VSV, 10^5 SV40-fibroblasts were plated in each well of a 24-well plate and infected at a MOI of 10 in DMEM supplemented with 2% FBS. The Stat-1–deficient patient has been described elsewhere (46). After 30 minutes, cells were washed and incubated in 500 μl of medium. All cells and supernatants were harvested and frozen at the time points indicated in the figures. Viral titers were determined by calculating the 50% end point ($TCID_{50}$), as described by Reed and Muench, after the inoculation of Vero cell cultures in 96-well plates. For HSV-1 replication, HSV-1 GFP (strain KOS) (49), at MOIs ranging from 0.1–10, was used to infect the 10^4 SV40 fibroblasts plated in 96-well plates. The GFP fluorescence of the samples was quantified after 24 hours. For assays of cell protection upon viral stimulation, cells were treated with IFN-α2b (Schering-Plough, 1×10^5 IU/ml) 18 hours before infection and during infection.

Cell viability assay

The viability of SV40-fibroblasts was assessed by resazurin oxidoreduction (TOX-8) (Sigma-Aldrich). Cells were plated in triplicate in 96-well flat-bottomed plates (2×10^4 cells/well) in DMEM supplemented with 2% FBS. Cells were infected with VSV or HSV-1 for 24 hours at the indicated MOI. Resazurin dye solution was then added, and the samples were incubated for an additional 2 hours at 37°C. Fluorescence was then measured at a wavelength of 590/560 nm. Background fluorescence, calculated for dye and complete medium alone (in the absence of cells), was then subtracted from the values for all the other samples; 100% viability corresponds to the fluorescence of uninfected cells. For assays of cell protection upon viral stimulation, cells were treated with IFN-α2b (Schering-Plough, 1×10^5 IU/ml) for 18 hours before infection and during infection.

Genome-wide transcriptional profile studies in fibroblasts and PBMCs

Microarray. SV40 fibroblasts obtained from patients or control subjects were stimulated with 25 μg/ml poly(I:C) or 20 ng/ml IL-1β or left unstimulated for 4 hours. Previously frozen PBMCs from patients or control subjects were left overnight in 10% FBS RPMI and then stimulated with 10 ng/ml LPS or 3 μg/ml R848 or left unstimulated for 2 hours. Total RNA was isolated (RNeasy Kit, Qiagen), and RNA integrity was assessed on an Agilent 2100 Bioanalyzer (Agilent). Biotinylated cRNA targets were prepared from 100 to 250 ng total RNA, using the Illumina TotalPrep RNA Amplification Kit (Ambion). The labelled cRNA (750 ng) were then incubated for 16 hours to HT-12 v4 BeadArrays (48,323 probes). Beadchip arrays were then washed, stained, and scanned on an Illumina HiScanSQ according to the manufacturer's instructions.

Data preprocessing. For the analysis of SV40 fibroblasts and PBMCs, after background subtraction, the raw signal values extracted with Illumina Beadstudio (version 2) were scaled using quantile normalization. Minimum intensity was set to 10, and all the intensity values were $\log_2$ transformed. Only the probes called present in at least 1 sample ($P < 0.01$) were retained for downstream analysis ($n = 23{,}281$ and $n = 22{,}881$ for fibroblasts and PBMCs, respectively).

Data analysis. Transcripts differentially regulated upon stimulation were defined based on a minimum 2-fold change (upregulation or downregulation) and a minimum absolute raw intensity difference of 100 with respect to the respective unstimulated sample. Heat maps were generated using R (version 2.12.2). Raw data from this study are available in the Gene Expression Omnibus repository (accession no. GSE32390; http://www.ncbi.nlm.nih.gov/gds).

DNA samples

Control gDNA samples were obtained from the CEPH for the 1,052 individuals from the CEPH-HGD panel. An additional 182 genomic samples were obtained from Prince Naif Center for Immunology Research, King Khalid University Hospital (KKUH), Riyadh, Saudi Arabia, for a panel of control Saudi Arabian children aged between 6 and 8 years old. This study was approved by the College of Medicine Research Council (CMRC) Ethical

Committee of the KKUH. Informed written consent was obtained from the patients' parents or guardians. The male-to-female ratio was approximately 2:1. In order to validate the P625L variant in a control Iranian population, we used 109 gDNA samples collected from healthy blood donors referred to the Medical Laboratories of the Arad General Hospital in Tehran. All individuals were from both sexes, from Tehran, and represent different ethnic groups, which are considered to be representative of the general Iranian population. DNA was extracted from whole blood. All data and the collection of samples were approved by the Iranian National Ethics Committee.

Statistics

Unless otherwise specified, mean values ± SEM were calculated for all results. The Student's *t* test (2 tailed) was used to determine significance, where $P < 0.05$ was found to be statistically significant.

Study approval

The experiments described here were conducted in France in accordance with local regulations approved by the CMRC Ethical Committee of the KKUH, the IRB of Necker Enfants Malades Hospital, and the IRB of Mofid Children Hospital.

Acknowledgments

We thank the members of the Laboratory of Human Genetics of Infectious Diseases, in particular Mélanie Migaud, Isabelle Melki, Martine Courat, Tony Leclerc, and Yelena Nemirovskaya; M. Oritz Lombardo for helpful discussions and technical assistance; Osamu Takeuchi for the dominant-negative TRIF vector; Sang Hoon Rhee for the doxycycline-inducible TRIF plasmid; Christopher Basler for the IFNB-luciferase plasmid; and Marianne Leruez for viral serology. We thank the children and their families for participating in this study. V. Sancho-Shimizu was supported by the Marie Curie Intra-European Fellowship 2008-2010. J.-L. Casanova was an international scholar of the Howard Hughes Medical Institute from 2005 to 2008. The Laboratory of Human Genetics of Infectious Diseases is supported by grants from the Agence national de la Recherche (ANR-08-MNP-014), The Rockefeller University Center for Clinical and Translational Science (grant no. 5UL1RR024143-03), and The Rockefeller University.

Received for publication May 31, 2011, and accepted in revised form October 6, 2011.

Address correspondence to: Vanessa Sancho-Shimizu, Faculty of Medicine Necker Hospital, 156 rue Vaugirard, 75015 Paris. Phone: 33.1.40.61.55.39; Fax: 33.1.40.61.56.88; E-mail: vanessa.sancho-shimizu@inserm.fr. Or to: Jean-Laurent Casanova, The Rockefeller University, 1230 York Avenue, New York, New York 10065, USA. Phone: 212.327.7331; Fax: 212.327.7330; E-mail: casanova@rockefeller.edu.

1. Whitley RJ. Herpes simplex virus in children. *Curr Treat Options Neurol.* 2002;4(3):231–237.
2. Whitley RJ, et al. Vidarabine versus acyclovir therapy in herpes simplex encephalitis. *N Engl J Med.* 1986;314(3):144–149.
3. Whitley RJ, Lakeman F. Herpes simplex virus infections of the central nervous system: therapeutic and diagnostic considerations. *Clin Infect Dis.* 1995; 20(2):414–420.
4. McGrath N, Anderson NE, Croxson MC, Powell KF. Herpes simplex encephalitis treated with acyclovir: diagnosis and long term outcome. *J Neurol Neurosurg Psychiatry.* 1997;63(3):321–326.
5. Gordon B, Selnes OA, Hart J Jr, Hanley DF, Whitley RJ. Long-term cognitive sequelae of acyclovir-treated herpes simplex encephalitis. *Arch Neurol.* 1990;47(6):646–647.
6. Sancho-Shimizu V, et al. Genetic susceptibility to herpes simplex virus 1 encephalitis in mice and humans. *Curr Opin Allergy Clin Immunol.* 2007;7(6):495–505.
7. Whitley RJ, Gnann JW. Viral encephalitis: familiar infections and emerging pathogens. *Lancet.* 2002;359(9305):507–513.
8. Abel L, et al. Age-dependent Mendelian predisposition to herpes simplex virus type 1 encephalitis in childhood. *J Pediatr.* 2010;157(4):623–629.
9. De Tiege X, Rozenberg F, Heron B. The spectrum of herpes simplex encephalitis in children. *Eur J Paediatr Neurol.* 2008;12(2):72–81.
10. Casrouge A, et al. Herpes simplex virus encephalitis in human UNC-93B deficiency. *Science.* 2006; 314(5797):308–312.
11. Zhang SY, et al. TLR3 deficiency in patients with herpes simplex encephalitis. *Science.* 2007; 317(5844):1522–1527.
12. Perez de Diego R, et al. Human TRAF3 adaptor molecule deficiency leads to impaired Toll-like receptor 3 response and susceptibility to herpes simplex encephalitis. *Immunity.* 2010;33(3):400–411.
13. Guo Y, et al. Herpes simplex virus encephalitis in a patient with complete TLR3 deficiency: TLR3 is otherwise redundant in protective immunity. *J Exp Med.* 2011;208(10):2083–2098.
14. Dupuis S, et al. Impaired response to interferon-alpha/beta and lethal viral disease in human STAT1 deficiency. *Nat Genet.* 2003;33(3):388–391.
15. Audry M, et al. NEMO is a key component of NF-κB- and IRF-3-dependent TLR3-mediated immunity to herpes simplex virus. *J Allergy Clin Immunol.* 2011;128(3):610–617.
16. Jouanguy E, et al. Human primary immunodeficiencies of type I interferons. *Biochimie.* 2007; 89(6–7):878–883.
17. Zhang SY, et al. Human Toll-like receptor-dependent induction of interferons in protective immunity to viruses. *Immunol Rev.* 2007;220:225–236.
18. Alcaïs A, Quintana-Murci L, Thaler DS, Schurr E, Abel L, Casanova JL. Life-threatening infectious diseases of childhood: single-gene inborn errors of immunity? *Ann N Y Acad Sci.* 2010;1214:18–33.
19. Matsumoto M, Kikkawa S, Kohase M, Miyake K, Seya T. Establishment of a monoclonal antibody against human Toll-like receptor 3 that blocks double-stranded RNA-mediated signaling. *Biochem Biophys Res Commun.* 2002;293(5):1364–1369.
20. Yamamoto M, et al. Cutting edge: a novel Toll/IL-1 receptor domain-containing adapter that preferentially activates the IFN-beta promoter in the Toll-like receptor signaling. *J Immunol.* 2002; 169(12):6668–6672.
21. Oshiumi H, Matsumoto M, Funami K, Akazawa T, Seya T. TICAM-1, an adaptor molecule that participates in Toll-like receptor 3-mediated interferon-beta induction. *Nat Immunol.* 2003;4(2):161–167.
22. Fitzgerald KA, et al. LPS-TLR4 signaling to IRF-3/7 and NF-kappaB involves the toll adapters TRAM and TRIF. *J Exp Med.* 2003;198(7):1043–1055.
23. Oshiumi H, et al. TIR-containing adapter molecule (TICAM)-2, a bridging adapter recruiting to toll-like receptor 4 TICAM-1 that induces interferon-beta. *J Biol Chem.* 2003;278(50):49751–49762.
24. Yamamoto M, et al. TRAM is specifically involved in the Toll-like receptor 4-mediated MyD88-independent signaling pathway. *Nat Immunol.* 2003; 4(11):1144–1150.
25. Yamamoto M, et al. Role of adaptor TRIF in the MyD88-independent toll-like receptor signaling pathway. *Science.* 2003;301(5633):640–643.
26. Hoebe K, et al. Identification of Lps2 as a key transducer of MyD88-independent TIR signalling. *Nature.* 2003;424(6950):743–748.
27. Zhang Z, et al. DDX1, DDX21, and DHX36 helicases form a complex with the adaptor molecule TRIF to sense dsRNA in dendritic cells. *Immunity.* 2011;34(6):866–878.
28. Jiang Z, Mak TW, Sen G, Li X. Toll-like receptor 3-mediated activation of NF-kappaB and IRF3 diverges at Toll-IL-1 receptor domain-containing adapter inducing IFN-beta. *Proc Natl Acad Sci U S A.* 2004;101(10):3533–3538.
29. Funami K, Sasai M, Oshiumi H, Seya T, Matsumoto M. Homo-oligomerization is essential for Toll/interleukin-1 receptor domain-containing adaptor molecule-1-mediated NF-kappaB and interferon regulatory factor-3 activation. *J Biol Chem.* 2008; 283(26):18283–18291.
30. Pichlmair A, et al. RIG-I-mediated antiviral responses to single-stranded RNA bearing 5′-phosphates. *Science.* 2006;314(5801):997–1001.
31. Meylan E, Tschopp J. Toll-like receptors and RNA helicases: two parallel ways to trigger antiviral responses. *Mol Cell.* 2006;22(5):561–569.
32. Yoneyama M, Fujita T. Function of RIG-I-like receptors in antiviral innate immunity. *J Biol Chem.* 2007;282(21):15315–15318.
33. Kaiser WJ, Offermann MK. Apoptosis induced by the toll-like receptor adaptor TRIF is dependent on its receptor interacting protein homotypic interaction motif. *J Immunol.* 2005;174(8):4942–4952.
34. Han KJ, et al. Mechanisms of the TRIF-induced interferon-stimulated response element and NF-kappaB activation and apoptosis pathways. *J Biol Chem.* 2004;279(15):15652–15661.
35. Funami K, et al. Spatiotemporal mobilization of Toll/IL-1 receptor domain-containing adaptor molecule-1 in response to dsRNA. *J Immunol.* 2007; 179(10):6867–6872.
36. Tatematsu M, et al. A molecular mechanism for Toll-IL-1 receptor domain-containing adaptor molecule-1-mediated IRF-3 activation. *J Biol Chem.* 2010; 285(26):20128–20136.
37. von Bernuth H, et al. Pyogenic bacterial infections in humans with MyD88 deficiency. *Science.* 2008;321(5889):691–696.
38. Picard C, et al. Pyogenic bacterial infections in humans with IRAK-4 deficiency. *Science.* 2003; 299(5615):2076–2079.
39. Ku CL, et al. IRAK4 and NEMO mutations in other-

wise healthy children with recurrent invasive pneumococcal disease. *J Med Genet.* 2007;44(1):16–23.
40. Casanova JL, Abel L, Quintana-Murci L. Human TLRs and IL-1Rs in host defense: natural insights from evolutionary, epidemiological, and clinical genetics. *Annu Rev Immunol.* 2011;29:447–491.
41. Yang K, et al. Human TLR-7–, -8–, and -9–mediated induction of IFN-alpha/beta and -lambda is IRAK-4 dependent and redundant for protective immunity to viruses. *Immunity.* 2005;23(5):465–478.
42. Ku CL, et al. Inherited disorders of human Toll-like receptor signaling: immunological implications. *Immunol Rev.* 2005;203:10–20.
43. Alcais A, Abel L, Casanova JL. Human genetics of infectious diseases: between proof of principle and paradigm. *J Clin Invest.* 2009;119(9):2506–2514.
44. Casanova JL, Abel L. Primary immunodeficiencies: a field in its infancy. *Science.* 2007;317(5838):617–619.
45. Barton ES, et al. Herpesvirus latency confers symbiotic protection from bacterial infection. *Nature.* 2007;447(7142):326–329.
46. Chapgier A, et al. Human complete Stat-1 deficiency is associated with defective type I and II IFN responses in vitro but immunity to some low virulence viruses in vivo. *J Immunol.* 2006;176(8):5078–5083.
47. Smahi A, et al. Genomic rearrangement in NEMO impairs NF-kappaB activation and is a cause of incontinentia pigmenti. The International Incontinentia Pigmenti (IP) Consortium. *Nature.* 2000; 405(6785):466–472.
48. Barde I, et al. Efficient control of gene expression in the hematopoietic system using a single Tet-on inducible lentiviral vector. *Mol Ther.* 2006;13(2):382–390.
49. Desai P, Person S. Incorporation of the green fluorescent protein into the herpes simplex virus type 1 capsid. *J Virol.* 1998;72(9):7563–7568.

OPEN ACCESS Freely available online

PLoS one

Phosphoinositide 3-Kinaseγ Controls the Intracellular Localization of CpG to Limit DNA-PKcs-Dependent IL-10 Production in Macrophages

Kaoru Hazeki[1]*, Yukiko Kametani[1], Hiroki Murakami[1], Masami Uehara[1], Yuki Ishikawa[1], Kiyomi Nigorikawa[1], Shunsuke Takasuga[2], Takehiko Sasaki[2], Tsukasa Seya[3], Misako Matsumoto[3], Osamu Hazeki[1]

1 Division of Molecular Medical Science, Graduate School of Biomedical Sciences, Hiroshima University, Hiroshima, Japan, **2** Department of Pathology and Immunology, Akita University School of Medicine, Akita, Japan, **3** Department of Microbiology and Immunology, Hokkaido University Graduate School of Medicine, Sapporo, Japan

Abstract

Synthetic oligodeoxynucleotides containing unmethylated CpG motifs (CpG) stimulate innate immune responses. Phosphoinositide 3-kinase (PI3K) has been implicated in CpG-induced immune activation; however, its precise role has not yet been clarified. CpG-induced production of IL-10 was dramatically increased in macrophages deficient in PI3Kγ ($p110\gamma^{-/-}$). By contrast, LPS-induced production of IL-10 was unchanged in the cells. CpG-induced, but not LPS-induced, IL-10 production was almost completely abolished in SCID mice having mutations in DNA-dependent protein kinase catalytic subunit (DNA-PKcs). Furthermore, wortmannin, an inhibitor of DNA-PKcs, completely inhibited CpG-induced IL-10 production, both in wild type and $p110\gamma^{-/-}$ cells. Microscopic analyses revealed that CpG preferentially localized with DNA-PKcs in $p110\gamma^{-/-}$ cells than in wild type cells. In addition, CpG was preferentially co-localized with the acidic lysosomal marker, LysoTracker, in $p110\gamma^{-/-}$ cells, and with an early endosome marker, EEA1, in wild type cells. Over-expression of p110γ in Cos7 cells resulted in decreased acidification of CpG containing endosome. A similar effect was reproduced using kinase-dead mutants, but not with a ras-binding site mutant, of p110γ. Thus, it is likely that p110γ, in a manner independent of its kinase activity, inhibits the acidification of CpG-containing endosomes. It is considered that increased acidification of CpG-containing endosomes in $p110\gamma^{-/-}$ cells enforces endosomal escape of CpG, which results in increased association of CpG with DNA-PKcs to up-regulate IL-10 production in macrophages.

Citation: Hazeki K, Kametani Y, Murakami H, Uehara M, Ishikawa Y, et al. (2011) Phosphoinositide 3-Kinaseγ Controls the Intracellular Localization of CpG to Limit DNA-PKcs-Dependent IL-10 Production in Macrophages. PLoS ONE 6(10): e26836. doi:10.1371/journal.pone.0026836

Editor: Jianming Qiu, University of Kansas Medical Center, United States of America

Received July 7, 2011; **Accepted** October 4, 2011; **Published** October 28, 2011

Funding: This work was supported by Grant-in-Aid for Scientific Research (C), KAKENHI20590060, 22590065 and 23590078, and Grant-in-Aid for Scientific Research on Innovative Areas, KAKENHI22114008. The funders had no role in study design, data collection and analysis, decision to publish, or preparation of the manuscript.

Competing Interests: The authors have declared that no competing interests exist.

* E-mail: khazeki@hiroshima-u.ac.jp

Introduction

Oligodeoxynucleotides containing unmethylated CpG motifs (CpG) are powerful immune adjuvants that induce the production of cytokines, including IL-6, IL-10, IL-12, IFN-α/β, and TNF-α [1,2]. Although previous studies have established that CpG-induced immune responses are mediated by endosomal TLR9 [3–5], cytoplasmic DNA-PKcs are also involved in CpG-signaling independent of TLR9 [6,7]. Thus, intracellular trafficking of CpG is critical to select downstream signaling molecules, which determine the cytokine species produced by macrophages [7,8].

Phosphoinositide 3-kinase (PI3K) has been reported to be both a positive and negative regulator of CpG-mediated cytokine production. CpG-induced IL-12 production is increased in plasmacytoid dendritic cells (pDC) from $p85\alpha^{-/-}$ mice, and by treatment of wild-type pDC with wortmannin [9]. Likewise, CpG-induced iNOS expression is increased by treating RAW264.7 cells with wortmannin [10]. By contrast, another group has reported that wortmannin inhibits CpG-induced production of IL-12, IL-6, TNF-α, and NO from RAW264.7 cells [11]. This inhibition has been considered to be the result of wortmannin-mediated disruption of class III PI3K signaling, which is responsible for CpG uptake [11]. Similarly, wortmannin inhibits CpG-induced IL-12 production by inhibiting CpG internalization in mouse-derived bone marrow cells [12]. In human pDC, another PI3K inhibitor, LY294002, also inhibits CpG-induced type I IFN production [13]. In this case, the uptake and endosomal trafficking of CpG are not affected, but nuclear translocation of IRF-7 was inhibited by LY294002, and also, by a specific inhibitor of PI3Kδ, IC87114 [13]. In addition, the PI3K/mTOR/p70S6K pathway plays a substantial role in the spatial interaction of TLR9/MyD88/IRF7, which is indispensable for the induction of type I IFN production by pDC [14]. These reports have indicated that PI3Ks play some roles in trafficking of CpG itself or its downstream molecules.

Pan- and/or some other specific PI3K inhibitors were used in all of the previous studies described above. All of these inhibitors bind competitively to the ATP binding pocket of PI3Ks and block kinase activity. Since DNA-dependent protein kinase catalytic

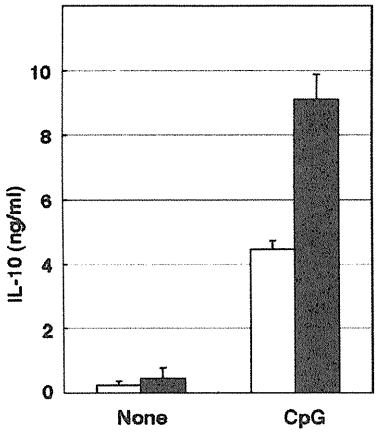

Figure 1. Increased IL-10 production following CpG stimulation of p110γ$^{-/-}$ cells. Macrophages from wild type (open bar) or p110γ$^{-/-}$ mice (solid bar) were incubated in 24-well plates with 10 ng/mL LPS, 200 ng/mL CpG, 50 μg/mL polyI:C or 200 nM Malp2 for 18 h. The amount of IL-10 in the medium was determined by ELISA. The values are the means ± SD of duplicate cultures from three independent experiments.
doi:10.1371/journal.pone.0026836.g001

subunit (DNA-PKcs) shares similar ATP binding site as a member of the PI3K-like kinase family, these inhibitors, even isoform-specific inhibitors, more or less inhibit DNA-PKcs [15]. This makes it difficult to elucidate the precise role of DNA-PKcs and PI3Ks in CpG-mediated cytokine production. In this paper, we used class IB PI3K (p110γ) knockout mice and SCID mice having mutations in DNA-PKcs to estimate their roles in CpG-mediated cytokine production. In agreement with a current report, DNA-PKcs play a substantial role in CpG-mediated IL-10 production in macrophages [7]. By contrast, p110γ specifically down-regulates IL-10 production following CpG-stimulation. Quantitative analysis of microscopic images showed that CpG localized preferentially with DNA-PKcs in the cytosol in p110γ$^{-/-}$ cells to a greater extent than in wild-type cells. We propose a novel regulatory role of p110γ in CpG-induced production of IL-10 through modulation of the intracellular trafficking of CpG.

Results

p110γ deficiency specifically increased IL-10 production upon CpG stimulation in macrophages

Mouse macrophages generated IL-10 in response to CpG (Fig. 1). Since PI3K has been implicated in the regulation of TLR-induced IL-10 production [16], we tested the effect of p110γ depletion on IL-10 production. CpG-induced IL-10 production was dramatically increased in macrophages from p110γ$^{-/-}$ mouse (Fig. 1). Although IL-10 production sometimes varied extremely between experiments, IL-10 production in wild type mice was always approximately half of that in p110γ$^{-/-}$ mice in each paired experiment. We also tested the cytokine production using macrophages from p85α$^{-/-}$ mice, and from p110δ$^{KD/KD}$ mice; neither displayed CpG-specific changes in IL-10 production similar to what was seen with p110γ$^{-/-}$ cells (data not shown).

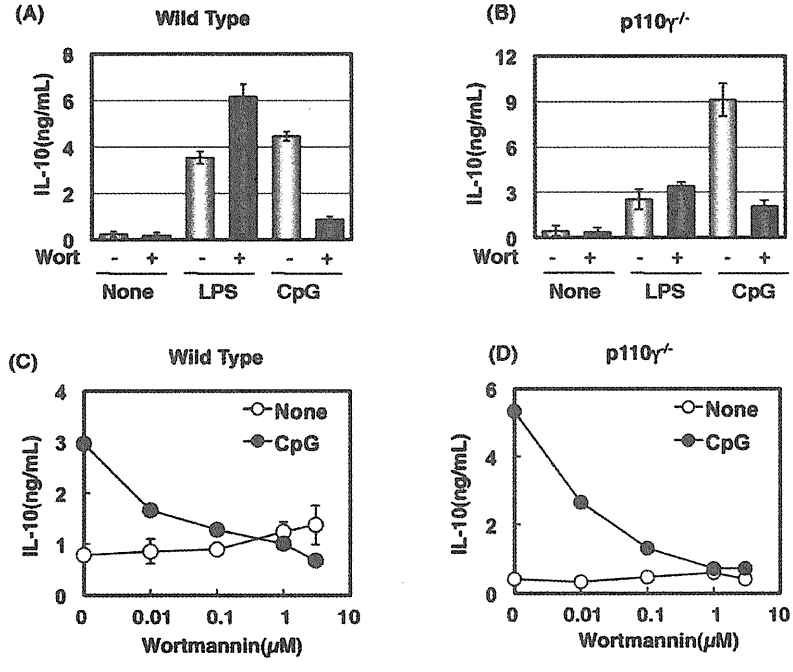

Figure 2. Inhibition of CpG-induced IL-10 production by wortmannin. Macrophages from wild type (A, C) or p110γ$^{-/-}$ mice (B, D) were pre-incubated with 0.1 μM (+ in A, B), or increasing concentration of wortmannin (C, D) for 15 min, followed by the addition of 10 ng/mL LPS (A, B) or 200 ng/mL CpG (A–D), for 18 h. The amount of IL-10 in the medium was determined by ELISA. The values are the means ± SD of duplicate cultures from three independent experiments.
doi:10.1371/journal.pone.0026836.g002

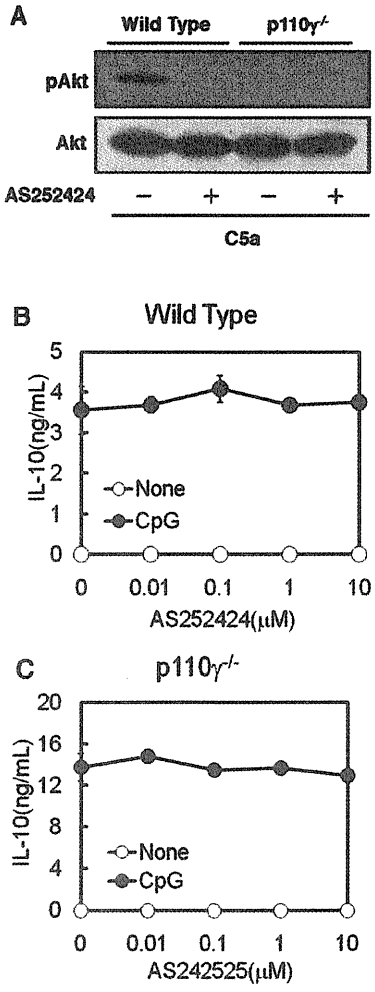

Figure 3. Irrelevance of the kinase activity of p110γ in the regulation of IL-10 production. (A) Macrophages from wild type or p110γ$^{-/-}$ mice were pre-incubated with 10 μM AS252424 for 15 min, followed by the addition of 100 ng/mL C5a for 5 min. Total cell lysates from the treated cells were analyzed by Western blot. (B and C) Macrophages from wild type (B) or p110γ$^{-/-}$ mice (C) were pre-incubated with increasing concentrations of AS252424 for 15 min, followed by the addition of 200 ng/mL CpG for 18 h. The amount of IL-10 in the medium was determined by ELISA. The values are the means ± SD of duplicate cultures from three independent experiments.
doi:10.1371/journal.pone.0026836.g003

Wortmannin inhibited IL-10 production induced by CpG, but increased that induced by LPS

Macrophages were treated with a pan-PI3K inhibitor, wortmannin. CpG-induced IL-10 production was almost completely inhibited by wortmannin while LPS-induced IL-10 production was rather increased in wild type cells (Fig. 2A). The effect of wortmannin on LPS-induced IL-10 production may be the result of the inhibition of p110γ, because the augmentation was not observed in p110γ$^{-/-}$ cells (Fig. 2B). However, wortmannin inhibited severely CpG-induced IL-10 production in p110γ$^{-/-}$ cells, as well as in wild type cells (Fig. 2C. D). The inhibition by wortmannin was specific to IL-10 production, because IL-12 production was unchanged by the treatment (data not shown).

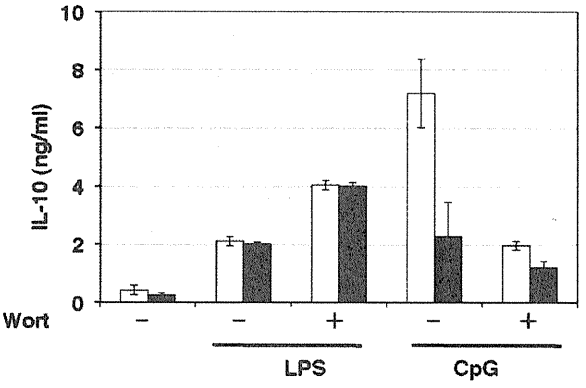

Figure 4. Failure of CpG to stimulate IL-10 production in SCID mice. Macrophages from wild type (open bar) or SCID (solid bar) mice were preincubated with 0.1 μM wortmannin (+) or vehicle (−) for 15 min, followed by the addition of 10 ng/mL LPS or 200 ng/mL CpG, for 18 h. The amount of IL-10 in the medium was determined by ELISA. The values are the means ± SD of duplicate cultures from three independent experiments.
doi:10.1371/journal.pone.0026836.g004

These data indicate that the target molecule of wortmannin responsible for the suppression of CpG-induced IL-10 was not p110γ.

p110γ-mediated negative regulation of IL-10 production was independent of kinase activity

Since a pan-PI3K inhibitor, wortmannin, did not mimic the effect of p110γ deficiency on CpG-induced IL-10 production, we next tested the effect of the p110γ-specific inhibitor, AS252424, on CpG-induced IL-10 production. C5a-induced Akt phosphorylation was completely abolished in p110γ$^{-/-}$ cells (Fig. 3A) [17]. The result confirmed that the C5a action is dependent on p110γ. AS252424 inhibited the C5a-induced Akt phosphorylation (Fig. 3A), indicating that the compound is a powerful tool for investigating the role of p110γ. Surprisingly, AS252424 did not cause an increase in CpG-induced IL-10 production in the wild type cells nor in p110γ$^{-/-}$ cells (Fig. 2B, C). These data suggest that the negative regulation of CpG-induced IL-10 production by p110γ was not dependent on its kinase activity.

CpG-induced IL-10 production was abolished in SCID mice

Recently, an indispensable role of DNA-PKcs in CpG-induced IL-10 production has been reported [7]. Since DNA-PKcs has a PI3K-like catalytic domain, the kinase activity is susceptible to wortmannin. As reported earlier [7], CpG-induced IL-10 production was defective in SCID mice (Fig. 4). Additionally, wortmannin inhibited significantly CpG-induced IL-10 production in wild type, whereas it did not affect this process in SCID mice (Fig. 4). This result suggests that wortmannin suppressed CpG-induced IL-10 production through inhibition of DNA-PKcs. By contrast, LPS-induced IL-10 production in SCID was identical to wild type with the same background mice (Fig. 4).

Co-localization of DNA-PKcs and CpG was increased in p110γ$^{-/-}$ cells

CpG is internalized via endocytosis and immediately moves into the lysosomal compartment [5,18,19]. A recent study reported that endosomal CpG preferentially induces IL-12 production, but,

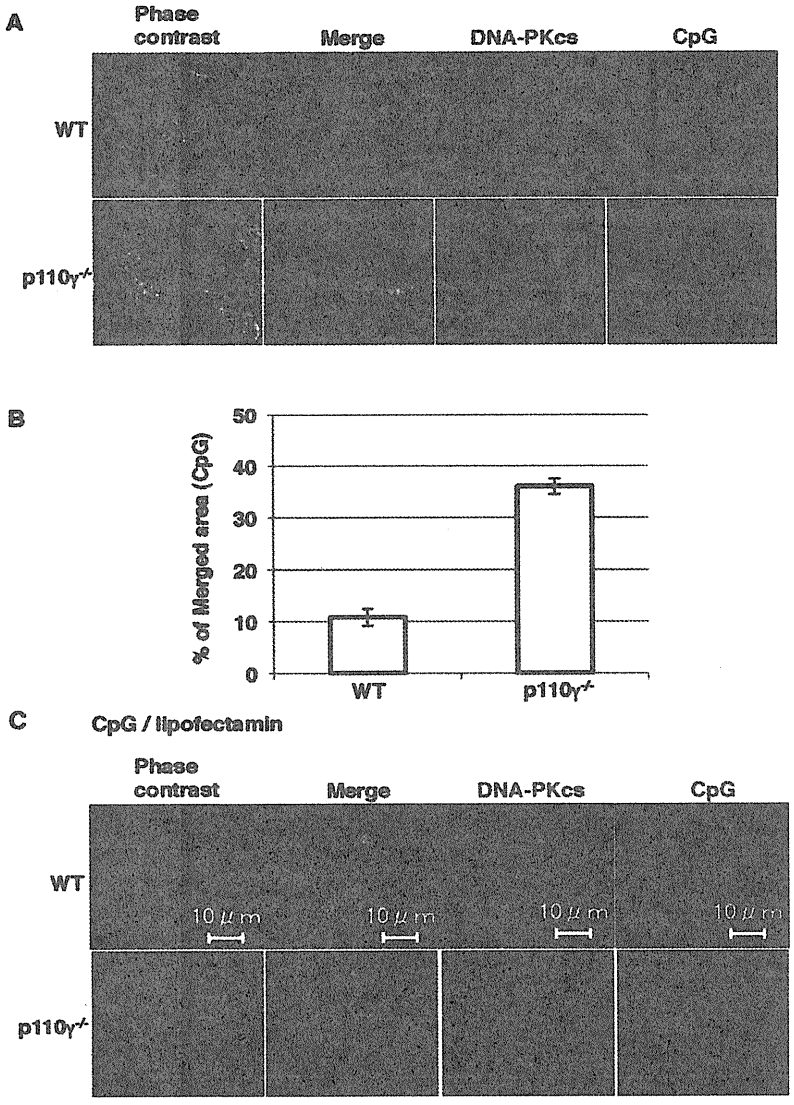

Figure 5. Increased co-localization of CpG and DNA-PKcs in p110γ$^{-/-}$ cells. Macrophages from wild type or p110γ$^{-/-}$ mice were incubated with 0.5 μM rhodamine-CpG (A) or rhodamine-CpG/lipofectamine LTX/Plus (C) for 60 min. The cells were washed, fixed, permeabilized, and stained with anti-DNA-PKcs antibody and Alexa 488-labeled secondary antibody. (B) The imaging data in (A) were quantified and shown as means ± SD.
doi:10.1371/journal.pone.0026836.g005

when released from the endosome, it associates with DNA-PKcs in cytoplasm and induces a greater amount of IL-10 [7]. Therefore, we hypothesized that CpG localized to the endosomal compartment in the wild type cells, and was more efficiently released into the cytosol in p110γ$^{-/-}$ cells. To quantify the co-localization of CpG and DNA-PKcs, macrophages were incubated with rhodamine-labeled CpG, fixed with formaldehyde, permeabilized, and incubated with anti-DNA-PKcs antibody. The merged area was calculated from the imaging data as described under materials and methods. The Co-localization area of CpG and DNA-PKcs was significantly increased in 110γ$^{-/-}$ cells (Fig. 5A, B). Interestingly, CpG complexed with cationic liposomes composed of Lipofectamine (LTX) and Plus reagent localized in large vesicles both in wild type and p110γ$^{-/-}$ cells, and scarcely co-localized with DNA-PKcs (Fig. 5C). Since wortmannin did not affect CpG uptake or localization of CpG or DNA-PKcs (data not shown), the PI3K inhibitor exclusively inhibits the kinase activity of DNA-PKcs.

Manipulation of CpG localization with cationic liposomes abolished the effect of p110γ deficiency on cytokine production

It seemed interesting to determine IL-10 production by CpG complexed with the lipofection reagent, which hardly co-localizes with DNA-PKcs. When cells were stimulated with this CpG/lipofection reagent, IL-10 production was decreased both in wild-type and p110γ$^{-/-}$ cells (Fig. 6). In addition, the augmentation of IL-10 production seen in p110γ$^{-/-}$ cells was completely abolished using this delivery system (Fig. 6).

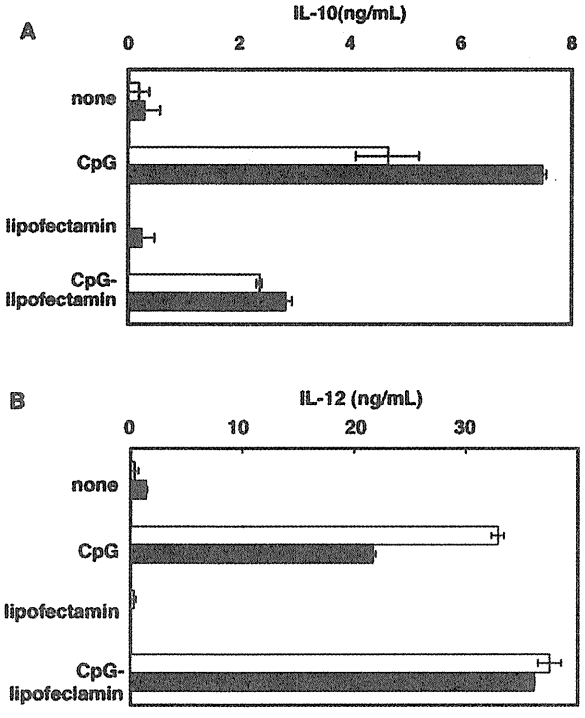

Figure 6. The effect of lipofection reagent on CpG-induced cytokine production. Macrophages from wild type (open bar) or p110γ$^{-/-}$ mice (solid bar) were incubated in 24-well plates with 200 ng/mL CpG or CpG/lipofectamine LTX/Plus reagent complex for 18 h. The amount of IL-10 (A) and IL-12 (B) in the medium was determined by ELISA. The values are the means ± SD of duplicate cultures from three independent experiments.
doi:10.1371/journal.pone.0026836.g006

CpG preferentially localized in the early endosome in wild type cells, and in lysosomes in p110γ$^{-/-}$ cells

We next tested the cellular delivery of CpG using an early endosome marker, EEA1, an endosome marker, dextran, and an acidic lysosome marker, LysoTracker. Quantitative analysis of microscopic images showed that more CpG merged with EEA1 and dextran in wild type cells than in p110γ$^{-/-}$ cells (Fig. 7A, B, D, E). By contrast, CpG preferentially merged with LysoTracker in p110γ$^{-/-}$ cells more than in wild-type cells (Fig. 7C, F). To further investigate the role of p110γ in CpG localization, Cos7 cells were transfected with p110γ and its mutant forms (unlike macrophages, Cos7 cells do not express p110γ). As shown in Fig. 8, most of the CpG was co-localized with LysoTracker in Cos7 cells transfected with vehicle alone, while scarcely co-localized with LysoTracker in the cells transfected with wild type p110γ. Interestingly, overexpression of a kinase-dead mutant of p110γ also inhibited the acidification of CpG-containing endosome. By contrast, the Ras-binding domain mutant form showed no effect on the CpG localization. These results suggest that PI3K p110γ play a role in endosomal acidification independent of its kinase activity. Since endosomal acidification is known to precede the endosomal leakage, acidification of CpG containing endosome may accelerate CpG translocation to the cytosol and the resultant association with DNA-PKcs to increase IL-10 production in macrophages.

CpG-induced but not LPS-induced IL-10 production was suppressed by inhibitors of endosomal acidification

Effect of chemical inhibitors of endosomal acidification [20] on CpG-induced IL-10 production was next examined. Both NH_4Cl and chloroquine strongly inhibited CpG-induced IL-10 production without affecting LPS-induced one (Fig. 9). The result supported our hypothesis that endosomal acidification is required for CpG-induced IL-10 production.

Discussion

In this study, we have identified a novel function of PI3K p110γ in the regulation of CpG localization. We have demonstrated this function using p110γ$^{-/-}$ macrophages and Cos7 cells transfected with p110γ. In macrophages, more CpG merged with the endosome markers, EEA1 and dextran, in wild type cells than in p110γ$^{-/-}$ cells, whereas preferentially merged with the acidic lysosome marker, LysoTracker, in p110γ$^{-/-}$ cells to a greater extent than in wild-type cells. In Cos7 cells, which do not express p110γ, most of the CpG was co-localized with LysoTracker, and scarcely co-localized with the dye in the cells transfected with p110γ. Another novel finding reported in this paper is that IL-10 production was increased specifically in p110γ$^{-/-}$ cells following CpG-stimulation. In p110γ$^{-/-}$ cells, the increased acidification of CpG containing endosomes and the resultant leakage of CpG to the cytosol, where DNA-PKcs resides, appears to be responsible for the modulation of cytokine production. For this reason, CpG-induced, but not LPS-induced, IL-10 production was almost completely abolished in SCID mice having mutations in DNA-PKcs. Furthermore, wortmannin, an inhibitor of DNA-PKcs, inhibited completely CpG-induced IL-10 production both in wild-type and in p110γ$^{-/-}$ cells. In addition to these, manipulation of the delivery system with cationic liposomes, which severely blocked the cytosolic delivery of CpG both in p110γ$^{-/-}$ and wild type cells, resulted in decreased IL-10 production. Finally, an intriguing point in this study is that the actions of p110γ on both the CpG delivery system and cytokine production were independent of its kinase activity.

Several kinase-independent functions of p110γ have been reported previously. Protein complexes containing p110γ are known to activate phosphodiesterase (PDE3B) in cardiomyocytes to degrade cAMP in a manner independent of its kinase activity [21,22]. Since increases in the cAMP level results in augmentation of TLR-mediated IL-12 production, with a decrease in IL-10 production [23], we had hypothesized that the increased IL-10 production in the absence of p110γ might be the result of elevated cAMP levels. To answer this question we tested some reagents known to increase cAMP, such as forskolin, prostaglandin E_2, 3-isobutyl-1-methylxanthin or dibutyryl cAMP in IL-10 production. Although these reagents more or less enhanced IL-10 production, the effect was not specific to CpG stimulation, but rather, was commonly observed in TLR-stimulation (data not shown). The other kinase-independent functions of p110γ are reported in vascular repair and platelet aggregation [22]. In addition, wild-type or the kinase-dead mutant of p110γ can block the growth of human colon cancer cells [24]. Although the mechanism of these kinase-independent actions of p110γ remains to be clarified, a scaffolding role for p110γ has been suggested [22].

p110γ$^{-/-}$ mice show severe defects in immune responses, and are protected completely against systemic anaphylaxis [25–28]. Additionally, in models of rheumatoid arthritis, systemic lupus erythematosus, and atherosclerosis, loss of p110γ activity results in protection against disease progression [29–31]. Since IL-10 is an anti-inflammatory cytokine, the increased IL-10 production in

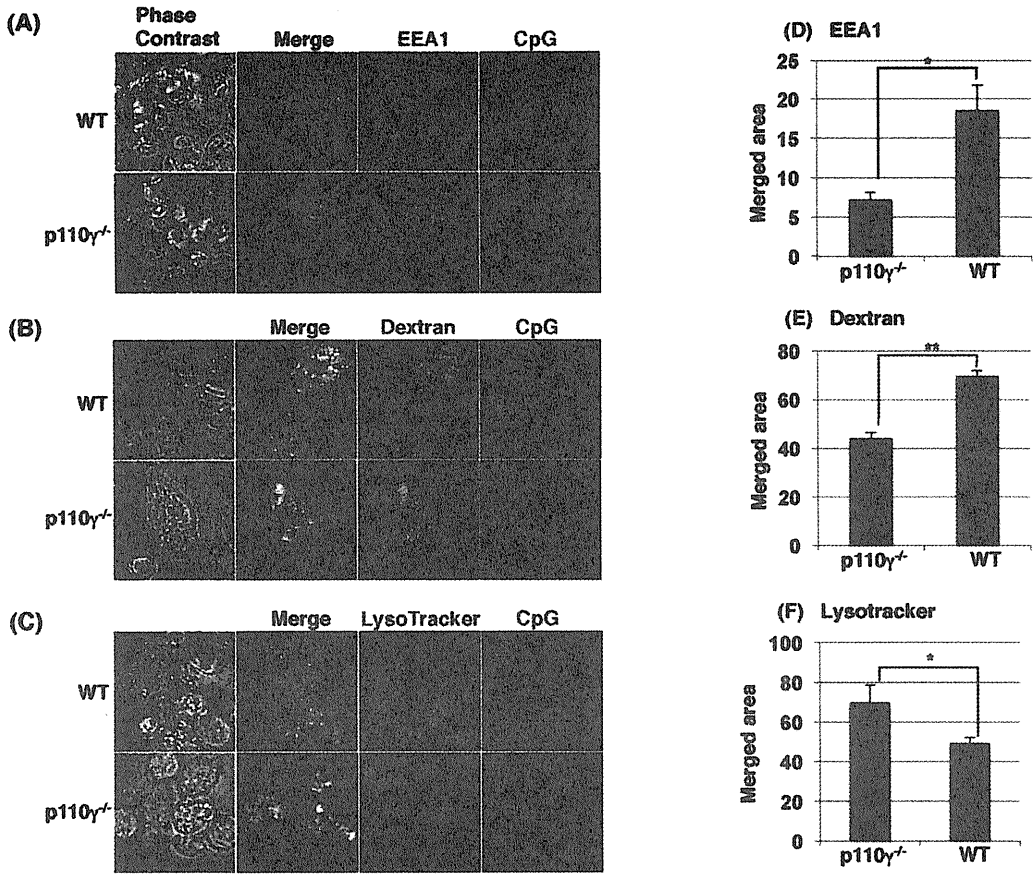

Figure 7. CpG localization in macrophages from wild type and p110γ$^{-/-}$ mice. Macrophages from wild type or p110γ$^{-/-}$ mice were incubated with 0.5 μM rhodamine-CpG (A, B) or FITC-CpG (C) for 30 min. FITC-dextran (1 mg/ml) (B) or LysoTracker red (50 nM) (C) was added simultaneously with CpG. The cells were washed and observed as live cells (B and C). In (A), the cells were fixed, permeabilized and stained with anti-EEA1 antibody and Alexa 488-labeled secondary antibody. The imaging data in (A, B, C) were quantified and shown as means ± SD in (D, E, F). *; $p<0.05$, **; $p<0.01$.
doi:10.1371/journal.pone.0026836.g007

p110γ-deficient cells may contribute, at least in a part, to protection against excessive inflammation. It is also likely that the increased IL-10 and decreased IL-12 production in p110γ$^{-/-}$ macrophage might explain partly the development of colorectal carcinomas in p110γ$^{-/-}$ mice [24], because the IL-12-mediated Th1 response favors effective anti-tumor immune responses [32]. Although further studies are needed to confirm the *in vivo* effect of p110γ on the translocation of CpG, our findings suggest that when p110γ is considered as a drug target for immune diseases [15,33,34], not only its lipid kinase function, but also its kinase-independent function should be considered.

Materials and Methods

Reagents

LPS (*E. coli* serotype 0111: B4), FITC-Dextran (average MW 40 kD) and C5a were from Sigma-Aldrich. Wortmannin was from Kyowa Medex (Tokyo, Japan). 5′-rhodamine-labeled, 5′-FITC-labeled and unlabeled CpG DNA (HPLC-purified phosphorothioate with the sequence of TCC ATG ACG TTC CTG ATG CT) were synthesized by Hokkaido System Science (Sapporo, Japan). LysoTracker Red was obtained from Lonza. Lipofectamine LTX Reagent, Plus Reagent and RPMI 1640 medium were from Invitrogen. The Protein Assay Kit was purchased from Bio-Rad. AS-252424 was from Cayman. Anti-pAkt (Ser473) antibody was from Cell Signalling, anti-Akt1/2 and anti-DNA-PKcs antibodies were from Santa Cruz, and anti-EEA1 was from GenScript. The IL-10 ELISA assay kit was from Biolegend.

Animals and cell isolation

All animal experiments were carried out in accordance with the NIH Guide for Care and Use of Laboratory Animals and approved by the animal care and use committee at Hiroshima University (Permit number: A08-23 and A08-46).

Female C57BL/6 mice, 8–12 weeks old, were purchased from Japan SLC, Inc. SCID, C.B-17/lcr$^{+/+}$, C.B-17/lcr-SCID/SCID mice were purchased from CLEA Japan. p110γ$^{-/-}$ mice on the C57BL/6 background were bred and maintained at Akita University (Akita, Japan). Thioglycollate-elicited macrophages were harvested from these mice. Briefly, mice were injected intra-peritoneally with 2 mL 3% thioglycollate broth. After 3 days, the peritoneal exudate cells were collected by washing the peritoneal cavity with ice-cold phosphate-buffered saline (PBS). The cells were seeded at about $5–10\times10^5$ cells/well in 24-well

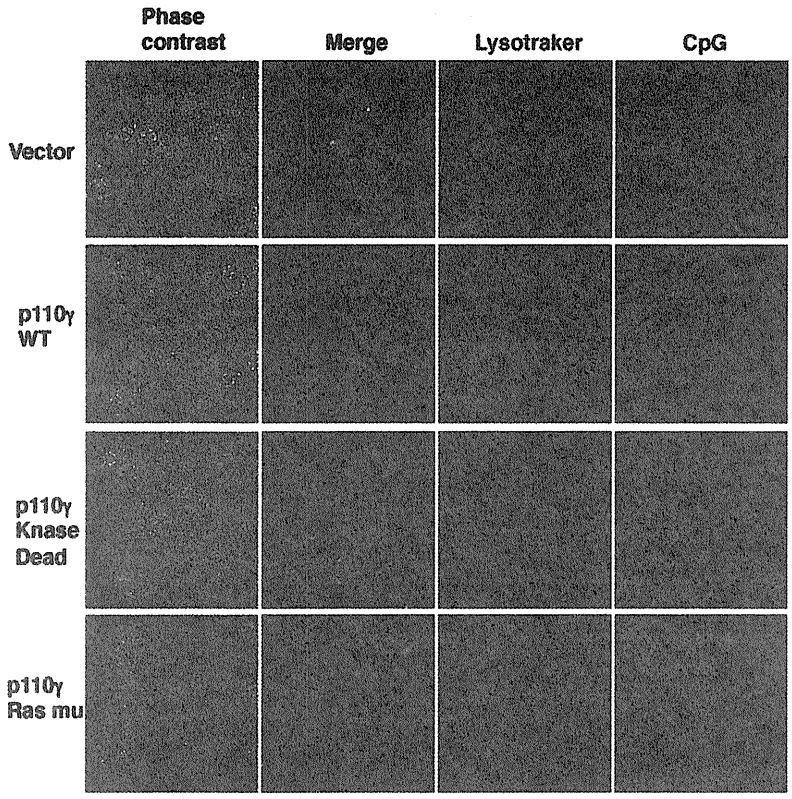

Figure 8. Effect of overexpression of p110γ on CpG localization in Cos7 cells. Cos7 cells were transfected with PI3K p110γor its mutant forms as described under materials and methods. Cells prepared in this manner were incubated with 50 nM LysoTracker red and 0.5 μM FITC-CpG for 30 min. The cells were washed and observed as live cells.
doi:10.1371/journal.pone.0026836.g008

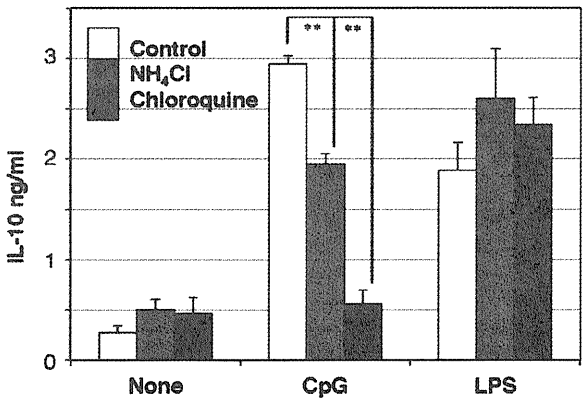

Figure 9. Effect of inhibitors of lysosomal acidification on IL-10 production. Macrophages from wild type mice were preincubated with 20 mM NH_4Cl, 50 μM Chloroquine or vehicle for 15 min, followed by the addition of 10 ng/mL LPS or 200 ng/mL CpG, for 18 h. The amount of IL-10 in the medium was determined by ELISA. The values are the means ± SD of duplicate cultures from three independent experiments. **; $p<0.01$.
doi:10.1371/journal.pone.0026836.g009

plates and incubated in humidified 5% CO_2 at 37°C for 1–2 h in RPMI 1640 medium supplemented with 10% fetal bovine serum (FBS) (MBL, Nagoya, Japan), to allow the cells to adhere to the wells. Non-adherent cells were removed by washing with PBS and the attached cells were used for experiments. Cos7 cells [35] were cultured in DMEM medium supplemented with 10% FBS.

Plasmids and transfection

Mammalian expression plasmids, pcDNA3 (Invitrogen), pcDNA3 containing wild-type p110γ, pcDNA3 containing a kinase-dead (R947P) mutant, or encoding a Ras binding site mutant (DASAA; T232D, K251A, K254S, K255A and K256A) [36] are transfected in to Cos7 cells using the Lipofectamine 2000 Reagent for 24 h.

Western blot

Cells were washed with PBS and lysed in 50 μL lysis buffer containing 25 mM Tris-HCl (pH 7.4), 0.5% Nonidet P-40, 150 mM NaCl, 1 mM sodium orthovanadate (Na_3VO_4), 1 mM EDTA, 0.1% BSA, 20 mM sodium fluoride, 1 mM phenylmethylsulfonyl fluoride, 2 μM leupeptin, 20 μM p-amidinophenylmethylsulfonyl fluoride, and 1 mM dithiothreitol. The cell lysates were centrifuged at 15,000 rpm for 10 min. Supernatants were collected and the protein concentration was determined using the Bio-Rad assay kit. Total cell lysates (100 μg protein) were mixed with 10 μL 5× sample buffer (62.5 mM Tris, pH 6.8, 1% SDS, 10% glycerol, 5% 2-mercaptoethanol, and 0.02% bromo-

phenol blue) and heated at 100°C for 5 min. The proteins were separated by SDS-PAGE and transferred electrophoretically onto a polyvinylidene difluoride (PVDF) membrane (Millipore). The membrane was blocked with 5% skim milk and incubated with the appropriate antibodies. Antibody binding was detected using a chemiluminescent substrate (Perkin-Elmer).

ELISA

Macrophage culture supernatants were used for the quantification of p40 and IL-10 using a commercially available ELISA kit.

Microscopy

Macrophages in multi-well, glass-bottom dishes (Greiner bio-one) were allowed to adhere for 60 min before the addition of rhodamine- or FITC-CpG. Where indicated, FITC-dextran or LysoTracker Red was added with CpG. The cells were washed four times to remove excess CpG before live cell imaging. Alternatively, the cells were fixed with 4% formaldehyde in PBS for 15 min, permeabilized with PBS containing 0.3% Triton X-100 and 0.5% BSA for 60 min, and incubated with anti-DNA-PKcs or anti-EEA1 at 4°C overnight. They were then incubated with Alexa 488-labeled goat anti-mouse IgG antibody $(Fab')_2$ for 2 h at room temperature. Cos7 cells were seeded into the culture wells a day before the transfection. The cells were incubated with LysoTracker red and FITC-CpG for 15 min as indicated. The cells were washed four times with PBS before imaging. Microscopic studies were performed using the Keyence BZ-9000 (Keyence, Osaka, Japan). The imaging data were analyzed by the BZ-H2A application. Values of (merged area)/(CpG area)×100 were determined from at least 5 imaging data, and the data are shown as the means ± SD. Statistical differences were determined at the level of $p<0.05$ or 0.01 with Student's t test.

Author Contributions

Conceived and designed the experiments: KH YK OH. Performed the experiments: KH YK HM MU YI. Analyzed the data: KH YK HM KN ST T. Seya MM OH. Contributed reagents/materials/analysis tools: KH ST T. Sasaki T. Seya. Wrote the paper: KH OH.

References

1. Krieg AM (2006) Therapeutic potential of Toll-like receptor 9 activation. Nat Rev Drug Discov 5: 471–484.
2. Wilson HL, Dar A, Napper SK, Marianela Lopez A, Babiuk LA, et al. (2006) Immune mechanisms and therapeutic potential of CpG oligodeoxynucleotides. Int Rev Immunol 25: 183–213.
3. Hemmi H, Takeuchi O, Kawai T, Kaisho T. Sato S, et al. (2000) A Toll-like receptor recognizes bacterial DNA. Nature 408: 740–745.
4. Bauer S, Kirschning CJ, Hacker H, Redecke V, Hausmann S, et al. (2001) Human TLR9 confers responsiveness to bacterial DNA via species-specific CpG motif recognition. Proc Natl Acad Sci U S A 98: 9237–9242.
5. Rutz M, Metzger J, Gellert T, Luppa P, Lipford GB, et al. (2004) Toll-like receptor 9 binds single-stranded CpG-DNA in a sequence- and pH-dependent manner. Eur J Immunol 34: 2541–2550.
6. Dragoi AM, Fu X, Ivanov S, Zhang P, Sheng L, et al. (2005) DNA-PKcs, but not TLR9, is required for activation of Akt by CpG-DNA. EMBO J 24: 779–789.
7. Yotsumoto S, Saegusa K, Aramaki Y (2008) Endosomal translocation of CpG-oligodeoxynucleotides inhibits DNA-PKcs-dependent IL-10 production in macrophages. J Immunol 180: 809–816.
8. Honda K, Ohba Y, Yanai H, Negishi H, Mizutani T, et al. (2005) Spatiotemporal regulation of MyD88-IRF-7 signalling for robust type-I interferon induction. Nature 434: 1035–1040.
9. Fukao T, Tanabe M, Terauchi Y, Ota T, Matsuda S, et al. (2002) PI3K-mediated negative feedback regulation of IL-12 production in DCs. Nat Immunol 3: 875–881.
10. Hazeki K, Kinoshita S, Matsumura T, Nigorikawa K, Kubo H, et al. (2006) Opposite effects of wortmannin and 2-(4-morpholinyl)-8-phenyl-1(4H)-benzopyran-4-one hydrochloride on toll-like receptor-mediated nitric oxide production: negative regulation of nuclear factor-{kappa}B by phosphoinositide 3-kinase. Mol Pharmacol 69: 1717–1724.
11. Kuo CC, Lin WT, Liang CM, Liang SM (2006) Class I and III phosphatidylinositol 3'-kinase play distinct roles in TLR signaling pathway. J Immunol 176: 5943–5949.
12. Ishii KJ, Takeshita F, Gursel I, Gursel M, Conover J, et al. (2002) Potential role of phosphatidylinositol 3 kinase, rather than DNA-dependent protein kinase, in CpG DNA-induced immune activation. J Exp Med 196: 269–274.
13. Guiducci C, Ghirelli C, Marloie-Provost MA, Matray T, Coffman RL, et al. (2008) PI3K is critical for the nuclear translocation of IRF-7 and type I IFN production by human plasmacytoid predendritic cells in response to TLR activation. J Exp Med 205: 315–322.
14. Cao W, Manicassamy S, Tang H, Kasturi SP, Pirani A, et al. (2008) Toll-like receptor-mediated induction of type I interferon in plasmacytoid dendritic cells requires the rapamycin-sensitive PI(3)K-mTOR-p70S6K pathway. Nat Immunol 9: 1157–1164.
15. Marone R, Cmiljanovic V, Giese B, Wymann MP (2008) Targeting phosphoinositide 3-kinase: moving towards therapy. Biochim Biophys Acta 1784: 159–185.
16. Saegusa K, Yotsumoto S, Kato S, Aramaki Y (2007) Phosphatidylinositol 3-kinase-mediated regulation of IL-10 and IL-12 production in macrophages stimulated with CpG oligodeoxynucleotide. Mol Immunol 44: 1323–1330.
17. Sasaki T, Irie-Sasaki J, Jones RG, Oliveira-dos-Santos AJ, Stanford WL, et al. (2000) Function of PI3Kgamma in thymocyte development, T cell activation, and neutrophil migration. Science 287: 1040–1046.
18. Hacker H, Mischak H, Miethke T, Liptay S, Schmid R, et al. (1998) CpG-DNA-specific activation of antigen-presenting cells requires stress kinase activity and is preceded by non-specific endocytosis and endosomal maturation. EMBO J 17: 6230–6240.
19. Latz E, Schoenemeyer A, Visintin A, Fitzgerald KA, Monks BG, et al. (2004) TLR9 signals after translocating from the ER to CpG DNA in the lysosome. Nat Immunol 5: 190–198.
20. Misinzo G, Delputte PL, Nauwynck HJ (2007) Inhibition of endosome-lysosome system acidication enhances porcine circovirus 2 infection of porcine epithelial cells. J Virol 82: 1128–1135.
21. Patrucco E, Notte A, Barberis L, Selvetella G, Maffei A, et al. (2004) PI3Kgamma modulates the cardiac response to chronic pressure overload by distinct kinase-dependent and -independent effects. Cell 118: 375–387.
22. Hirsch E, Braccini L, Ciraolo E, Morello F, Perino A (2009) Twice upon a time: PI3K's secret double life exposed. Trends Biochem Sci 34: 244–248.
23. Koga K, Takaesu G, Yoshida R, Nakaya M, Kobayashi T, et al. (2009) Cyclic adenosine monophosphate suppresses the transcription of proinflammatory cytokines via the phosphorylated c-Fos protein. Immunity 30: 372–383.
24. Sasaki T, Irie-Sasaki J, Horie Y, Bachmaier K, Fata JE, et al. (2000) Colorectal carcinomas in mice lacking the catalytic subunit of PI(3)Kgamma. Nature 406: 897–902.
25. Suire S, Coadwell J, Ferguson GJ, Davidson K, Hawkins P, et al. (2005) p84, a new Gbetagamma-activated regulatory subunit of the type IB phosphoinositide 3-kinase p110gamma. Curr Biol 15: 566–570.
26. Voigt P, Dorner MB, Schaefer M (2006) Characterization of p87PIKAP, a novel regulatory subunit of phosphoinositide 3-kinase gamma that is highly expressed in heart and interacts with PDE3B. J Biol Chem 281: 9977–9986.
27. Stephens LR, Eguinoa A, Erdjument-Bromage H, Lui M, Cooke F, et al. (1997) The G beta gamma sensitivity of a PI3K is dependent upon a tightly associated adaptor, p101. Cell 89: 105–114.
28. Rommel C, Camps M, Ji H (2007) PI3K delta and PI3K gamma: partners in crime in inflammation in rheumatoid arthritis and beyond? Nat Rev Immunol 7: 191–201.
29. Barber DF, Bartolome A, Hernandez C, Flores JM, Redondo C, et al. (2005) PI3Kgamma inhibition blocks glomerulonephritis and extends lifespan in a mouse model of systemic lupus. Nat Med 11: 933–935.
30. Chang JD, Sukhova GK, Libby P, Schvartz E, Lichtenstein AH, et al. (2007) Deletion of the phosphoinositide 3-kinase p110gamma gene attenuates murine atherosclerosis. Proc Natl Acad Sci U S A 104: 8077–8082.
31. Camps M, Ruckle T, Ji H, Ardissone V, Rintelen F, et al. (2005) Blockade of PI3Kgamma suppresses joint inflammation and damage in mouse models of rheumatoid arthritis. Nat Med 11: 936–943.
32. Fukao T, Koyasu S (2003) PI3K and negative regulation of TLR signaling. Trends Immunol 24: 358–363.
33. Ohashi PS, Woodgett JR (2005) Modulating autoimmunity: pick your PI3 kinase. Nat Med 11: 924–925.
34. Ruckle T, Schwarz MK, Rommel C (2006) PI3Kgamma inhibition: towards an 'aspirin of the 21st century'? Nat Rev Drug Discov 5: 903–918.
35. Gluzman Y (1981) SV40-transformed simian cells support the replication of early SV40 mutants. Cell 23: 175–182.
36. Suire S, Condliffe AM, Ferguson GJ, Ellson CD, Guillou H, et al. (2006) Gbetagammas and the Ras binding domain of p110gamma are both important regulators of PI(3)Kgamma signalling in neutrophils. Nat Cell Biol 8: 1303–1309.

The TLR3/TICAM-1 Pathway Is Mandatory for Innate Immune Responses to Poliovirus Infection

Hiroyuki Oshiumi,*,[1] Masaaki Okamoto,*,[1] Ken Fujii,[†] Takashi Kawanishi,* Misako Matsumoto,* Satoshi Koike,[†] and Tsukasa Seya*

Cytoplasmic and endosomal RNA sensors recognize RNA virus infection and signals to protect host cells by inducing type I IFN. The cytoplasmic RNA sensors, retinoic acid inducible gene I/melanoma differentiation-associated gene 5, actually play pivotal roles in sensing virus replication. IFN-β promoter stimulator-1 (IPS-1) is their common adaptor for IFN-inducing signaling. Toll/IL-1R homology domain-containing adaptor molecule 1 (TICAM-1), also known as TRIF, is the adaptor for TLR3 that recognizes viral dsRNA in the early endosome in dendritic cells and macrophages. Poliovirus (PV) belongs to the Picornaviridae, and melanoma differentiation-associated gene 5 reportedly detects replication of picornaviruses, leading to the induction of type I IFN. In this study, we present evidence that the TLR3/TICAM-1 pathway governs IFN induction and host protection against PV infection. Using human PVR transgenic (PVRtg) mice, as well as IPS-$1^{-/-}$ and TICAM-$1^{-/-}$ mice, we found that TICAM-1 is essential for antiviral responses that suppress PV infection. TICAM-$1^{-/-}$ mice in the PVRtg background became markedly susceptible to PV, and their survival rates were decreased compared with wild-type or IPS-$1^{-/-}$ mice. Similarly, serum and organ IFN levels were markedly reduced in TICAM-$1^{-/-}$/PVRtg mice, particularly in the spleen and spinal cord. The sources of type I IFN were CD8α^{+}/CD11c^{+} splenic dendritic cells and macrophages, where the TICAM-1 pathway was more crucial for PV-derived IFN induction than was the IPS-1 pathway in ex vivo and in vitro analyses. These data indicate that the TLR3/TICAM-1 pathway functions are dominant in host protection and innate immune responses against PV infection. ***The Journal of Immunology*, 2011, 187: 5320–5327.**

When RNA viruses infect mammalian cells, type I IFN is generated to suppress viral infection. IFN-inducing pathways evoked by viral dsRNA have been identified in humans and mice, and the possible involvement of these pathways in protection against viruses has been examined using gene-disrupted mice and various virus species (1). The sensing of dsRNA by the innate immune system is accomplished either by TLR3 or by cytoplasmic sensors such as dsRNA-dependent protein kinase (so-called PKR), retinoic acid inducible gene I (RIG-I), and melanoma differentiation-associated gene 5 (MDA5) (2). In virus-infected cells, RIG-I and MDA5 mainly participate in type I IFN induction in conjunction with the adaptor molecule IFN-β promoter stimulator-1 (IPS-1; also known as MAVS, Cardif, or VISA) (1). The role of these molecules in host cell protection has been clearly delineated in RNA virus infection.

Toll/IL-1R homology domain-containing adaptor molecule 1 (TICAM-1; also called TRIF) is the adaptor of TLR3 (3–5). When TLR3 senses dsRNA on the endosomal membrane, it induces type I IFN (6, 7). The adaptor TICAM-1 plays a pivotal role in TLR3-mediated IFN-α/β induction. Once dsRNA stimulates TLR3, TICAM-1 transiently couples with TLR3 and forms a multimer, translocating to a distinct region of the cytoplasm (8). In its multimeric form, TICAM-1 recruits the kinase complex to activate IFN regulatory factors (IRF)-3 and -7, which induce type I IFN production (7, 9). Historically, this IFN-inducing pathway was identified earlier than the cytoplasmic RIG-I/MDA5 pathway (10, 11). Many reports have mentioned the possibility that the TLR3/TICAM-1 pathway is involved in the anti-viral IFN response (12), but no definitive evidence of the anti-viral properties of this pathway has been obtained using TICAM-$1^{-/-}$ mice (13). Only a DNA virus, mouse CMV (MCMV), has been shown to infect TICAM-$1^{-/-}$ mice, and thus mouse cells are partly protected from MCMV by the TICAM-1 pathway (5, 14).

Poliovirus (PV) is a positive strand ssRNA virus that produces dsRNA intermediates during viral replication (15), modified with 5′ terminal Vpg protein (16), a characteristic feature of picornaviruses. It is generally accepted that picornaviruses are recognized by MDA5 but not RIG-I in infected cells, presumably due to the generation of this unusual dsRNA. This concept was confirmed by the finding that MDA5$^{-/-}$ mice fail to induce type I IFN in response to encephalomyocarditis virus (EMCV) and permit severe EMCV infection (13, 17). However, another picornavirus, coxsackie B virus (CBV) serotype 3, is recognized by TLR3 in infected cells and induces IFN-γ as an effector for suppressing CBV infection

*Department of Microbiology and Immunology, Hokkaido University Graduate School of Medicine, Sapporo 060-8638, Japan; and [†]Department of Microbiology and Immunology, Tokyo Metropolitan Institute for Neuroscience, Tokyo Metropolitan Organization for Medical Research, Tokyo 156-0057, Japan

[1]H.O. and M.O. contributed equally to this work.

Received for publication May 24, 2011. Accepted for publication September 6, 2011.

This work was supported in part by Grants-in-Aid from the Ministry of Education, Science, and Culture of Japan (Specified Project for Advanced Research), the Ministry of Health, Labor, and Welfare of Japan, the Takeda Foundation, and by the Waxmann Foundation. Financial support by the Program of Founding Research Centers for Emerging and Reemerging Infectious Diseases, Ministry of Education, Culture, Sports, Science, and Technology of Japan, is gratefully acknowledged.

Address correspondence and reprint requests to Prof. Tsukasa Seya, Department of Microbiology and Immunology, Graduate School of Medicine, Hokkaido University, Kita-ku, Kita-15 Nishi-17, Sapporo, Hokkaido 060-8638, Japan. E-mail address: seya-tu@pop.med.hokudai.ac.jp

The online version of this article contains supplemental material.

Abbreviations used in this article: BM, bone marrow; BM-DC, bone marrow-derived dendritic cell; BM-Mf, bone marrow-derived macrophage; CBV, coxsackie B virus; DC, dendritic cell; EMCV, encephalomyocarditis virus; HCV, hepatitis C virus; IFIT-1, IFN-induced protein with tetratripeptide repeats 1; IP-10, IFN-γ–induced protein 10; IPS-1, IFN-β promoter stimulator-1; IRF, IFN regulatory factor; KO, knockout; MCMV, mouse cytomegalovirus; MDA5, melanoma differentiation-associated gene 5; MEF, mouse embryonic fibroblast; Mf, macrophage; MOI, multiplicity of infection; PV, poliovirus; PVRtg, poliovirus receptor transgenic; RIG-I, retinoic acid inducible gene I; RT-qPCR, real-time quantitative PCR; TICAM-1, Toll/IL-1R homology domain-containing adaptor molecule 1; WNV, West Nile virus; WT, wild-type.

www.jimmunol.org/cgi/doi/10.4049/jimmunol.1101503

(18). In this study, we analyzed in vivo infection of a popular picornavirus, PV, using PVR transgenic (PVRtg) mice, which show a neurotropic phenotype during PV infection similar to humans (19, 20). Using this mouse model, in combination with TICAM-1$^{-/-}$ or IPS-1$^{-/-}$ mice, we present evidence that the host TICAM-1 pathway, particularly in macrophages (Mf), serves as a source of type I IFN induction and protects host PVRtg mice from PV infection and paralytic death. Thus, the strategy for host protection against picornaviruses is not simply based on the MDA5-dependent dsRNA recognition, but is variable depending on picornavirus species.

Materials and Methods

Mice

All mice were backcrossed with C57BL/6 mice more than seven times before use. TICAM-1$^{-/-}$ (21) and IPS-1$^{-/-}$ mice (this study) were generated in our laboratory. TLR3$^{-/-}$ (4), IRF-3$^{-/-}$, and IRF-7$^{-/-}$ mice (22) were provided by Drs. S. Akira (Osaka University, Osaka, Japan) and T. Taniguchi (University of Tokyo, Tokyo, Japan). PVRtg mice were provided as reported previously (20). All mice were maintained under specific pathogen-free conditions in the Animal Facility at Hokkaido University Graduate School of Medicine (Sapporo, Japan). Animal experiments were performed according to the guidelines set by the Animal Safety Center, Japan.

Generation of IPS-1–deficient mice

The *IPS-1* gene was amplified by PCR using genomic DNA extracted from embryonic stem cells. The targeting vector was constructed by replacing the second and third exons with a neomycin-resistance gene cassette (Neo), and an HSV thymidine kinase driven by the PGK promoter was inserted into the genomic fragment for negative selection. After the targeting vector was transfected into 129/Sv mice-derived embryonic stem cells, G418 and ganciclovir doubly resistant colonies were selected and screened by PCR. The targeted cell line was injected into C57BL/6 blastocysts, resulting in the birth of male chimeric mice. These mice were then backcrossed with C57BL/6 mice. The disruption of the *IPS-1* gene was confirmed by PCR for the long and short arms. The abolishment of IPS-1 mRNA expression was confirmed by real-time quantitative PCR (RT-qPCR).

Cells, viruses, and reagents

Wild-type (WT) and TICAM-1$^{-/-}$ mouse embryonic fibroblasts (MEF) were prepared from 12.5- to 13.5-d-old embryos. PV, strain Mahoney, was amplified in Vero cells, and the viral titer was determined by a plaque assay. Bone marrow (BM) cells were prepared from the femur and tibia. The cells were cultured in RPMI 1640 (Invitrogen, New York, NY) supplemented with 10% FCS, 100 μM 2-ME, and 10 ng/ml murine GM-CSF or the culture supernatant of NIH3T3 cells expressing M-CSF. After 6 d, cells were collected and used as bone marrow-derived dendritic cells (BM-DC) or BM-derived macrophages (BM-Mf). For the preparation of BM-DC and BM-Mf, the medium was changed every 2 d. Splenic DC and NK cells were isolated using the MACS system (Miltenyi Biotec, Auburn, CA).

Experimental infection of mice

Five- to 8-wk-old C57BL/6 female mice were used throughout this study. Mice of different genotypes were i.p. or i.v. infected with PV at the doses indicated. The viability of the infected mice was monitored for 2 wk. We collected sera from the mice at different time points to measure viral titers by a plaque assay and cytokine levels by an ELISA. To determine the tissue viral titer, mice were euthanized and organs were aseptically removed and frozen by liquid nitrogen. Because the organs were not perfused before organs were removed, virus titers were determined including blood. Specimens were homogenized in 2 ml PBS on ice, and titers were determined by a plaque assay.

ELISA

Culture supernatants of cells (10^5) seeded on 24-well plates or sera were collected and analyzed for cytokine levels with ELISA. ELISA kits for IFN-α and IFN-β were purchased from PBL Biomedical Laboratories. ELISA was performed according to the manufacturer's instructions.

qPCR

For qPCR, total RNA was extracted with TRIzol (Invitrogen), and 0.2–0.5 μg RNA was reverse-transcribed using a high-capacity cDNA transcription kit (Applied Biosystems, Piscataway, NJ) with random primers according to the manufacturer's instructions. qPCR was performed using a Step One real-time PCR system (Applied Biosystems).

In vivo blocking of NK activity

Mice (PVRtg and PVRtg/TICAM-1$^{-/-}$) were i.p. injected with 250 μg anti-NK1.1 Ab, asialoGM1 Ab, or control PBS as described previously (21). One day later, the mice were i.p. inoculated with 10^4 PFU PV. One to 7 d after PV injection, depletion of peripheral NK1.1$^+$ cells was confirmed by flow cytometry. Then, the mortality of the mice was monitored. In some experiments, the spleen cells were harvested and NK cells (DX5$^+$ cells) were positively isolated using the MACS system (Miltenyi Biotec). The DX5$^+$ NK cells were suspended in RPMI 1640 containing 10% FCS and mixed with ^{51}Cr-labeled B16D8 cells at the indicated E:T ratios. After 4 h, the supernatants were harvested and [^{51}Cr] release was measured.

Statistical analysis

Statistical significance of differences between groups was determined by the Student *t* test, and survival curves were analyzed by the log-rank test using Prism 4 for Macintosh software (GraphPad Software). Student *t* tests and χ^2 goodness-of-fit tests were performed using Microsoft Excel software and a χ^2 distribution table.

Results

TICAM-1 is essential for protection of PVRtg mice against PV infection

Mice lacking the *mda-5* gene abrogate the production of type I IFN in response to EMCV infection and are more susceptible to infection with EMCV (13, 17). Because EMCV is a picornavirus, it has been proposed that MDA5 is critical for sensing picornavirus infection. In infected cells, picornaviruses efficiently generate long dsRNA, which is recognized by the cytoplasmic dsRNA sensor MDA5 (23). The 5′ end of the PV genomic RNA is linked to a VPg protein (16), not to a 5′-triphosphate, a major ligand for another cytoplasmic RNA sensor, RIG-I (24, 25). Thus, we first tested, using the PVRtg mouse model (20), whether the mortality of PV-infected mice is affected by disruption of IPS-1 (Fig. 1*A*). Approximately 70% of WT (PVRtg) mice and ~40% of IPS-1$^{-/-}$ mice survived >10 d postinoculation at an i.p. dose of 2×10^4 PFU. No statistical significance between these two groups was detected (Fig. 1*A*). In the same experiments, TICAM-1$^{-/-}$ mice died within 5 d by paralysis (Fig. 1*B*).

We next investigated the effect of the route of PV infection on mortality in this mouse model. PV (2×10^3 PFU) was injected i.p. or i.v. into WT and TICAM-1 mice and their mortality was examined (Fig. 1*C*, 1*D*). All TICAM-1$^{-/-}$ mice died by paralysis within 7.5 d irrespective of the injection route. The significance of this early mortality rate of PV-infected TICAM-1$^{-/-}$ mice was supported by statistical analysis. The mortality rates were slightly high in WT mice compared with IPS-1$^{-/-}$ mice when PV loads in mice were not very high (Supplemental Fig. 1*A*). This tendency seemingly diminished by early death of IPS-1$^{-/-}$ mice with high doses of PV input. These data suggested that TICAM-1, rather than IPS-1 (or the sensors RIG-I and MDA5), is a critical factor in protecting mice from PV-mediated paralytic death. This conclusion was confirmed using RIG-I$^{-/-}$ and MDA5$^{-/-}$ mice with a PVRtg background (S. Abe, K. Fujii, and S. Koike, submitted for publication).

These results showed a discrepancy with previous indications that MDA5 is critical in picornavirus protection (13). We therefore tested the dose dependence of PV in the survival of WT versus TICAM-1$^{-/-}$ mice. Surprisingly, high doses of PV (2×10^5 and 2×10^6 PFU) induced paralytic death in all WT as well as TICAM-1$^{-/-}$ mice within 6 d (Fig. 2*A*, 2*B*). Thus, high doses of PV (>2×10^5 PFU) appear to overpower the TICAM-1 PV-protective activity in vivo, which confirmed previous findings using other picornaviruses (13). TICAM-1 was most effective in